Research Square

Preprints are preliminary reports that have not undergone peer review.
They should not be considered conclusive, used to inform clinical practice,
or referenced by the media as validated information.

TM7SF3 Drives PI3K/AKT-mediated CX3CL1 Secretion to Promote Macrophage M2 Polarization in Gastric Cancer

Ran Shen

1327494612@qq.com

Southern Medical University First Affiliated Hospital: Southern Medical University Nanfang Hospital
https://orcid.org/0009-0001-2543-1689

Qianhui Zheng

Southern Medical University First Affiliated Hospital: Southern Medical University Nanfang Hospital

Donghua Huang

Southern Medical University First Affiliated Hospital: Southern Medical University Nanfang Hospital

Zhou Xu

Southern Medical University First Affiliated Hospital: Southern Medical University Nanfang Hospital

Mo You

Southern Medical University First Affiliated Hospital: Southern Medical University Nanfang Hospital

Jiayong He

Southern Medical University First Affiliated Hospital: Southern Medical University Nanfang Hospital

Zhe Wang

Southern Medical University First Affiliated Hospital: Southern Medical University Nanfang Hospital

Xiaoyan Li

Ganzhou People's Hospital

Caixiu Mo

Shenzhen University General Hospital

Zhenghong Lu

Southern Medical University First Affiliated Hospital: Southern Medical University Nanfang Hospital

Hao Liu

Southern Medical University First Affiliated Hospital: Southern Medical University Nanfang Hospital

Zhenzhan Zhang

Southern Medical University First Affiliated Hospital: Southern Medical University Nanfang Hospital

Guoxin Li

Southern Medical University First Affiliated Hospital: Southern Medical University Nanfang Hospital

Research Article

Keywords: TM7SF3, Immune infiltration, Trametinib, Macrophages, GC

Posted Date: November 1st, 2026

DOI: https://doi.org/10.21203/rs.3.rs-10763784/v1

License: This work is licensed under a Creative Commons Attribution 4.0 International License.
Read Full License

Abstract

Background

Gastric cancer (GC) remains one of the leading causes of cancer-related mortality worldwide, macrophage is a contributor to tumor progression and resistance to immunotherapy. Transmembrane 7 superfamily member 3 (TM7SF3) has been implicated in cellular stress responses, but its immune function remain unknown in GC.

Methods

TM7SF3 expression and its clinical significance were comprehensively analyzed using different datasets and validated in human GC specimens. Gain- and loss-of-function assays were performed in human and murine GC cell lines to evaluate cell proliferation, migration and apoptosis viability. Macrophage polarization was assessed by using conditioned medium-induced THP-1-derived macrophages, bone marrow-derived macrophages and xenograft models. Pharmacological inhibition/activation assays were used to investigate the underlying mechanism. Patient-derived organoids and xenograft models were used to evaluate the efficacy of anti-PD-1 immunotherapy in combination with Trametinib.

Results

TM7SF3 was significantly upregulated in GC tissues and was associated with advanced tumor stage and poor prognosis. Functionally, TM7SF3 promoted GC cell proliferation and migration while suppressing apoptosis. Mechanistically, TM7SF3 activated the downsteam PI3K/AKT signaling pathway, resulting in increased CX3CL1 expression and secretion, which subsequently promoted macrophage M2 polarization. Inhibition of PI3K/AKT pathway abolished TM7SF3-induced CX3CL1 expression and secretion, which induce M2 macrophage polarization, whereas AKT activation partially rescued these effects. Clinically, efficacy of Trametinib was found to depend on TM7SF3 expression level and was exhibited by patient-derived organoids model in vitro. The antitumor activity of anti-PD-1 therapy in combination with Trametinib was further enhanced in TM7SF3-overexpressed GC cells in vivo.

Conclusion

TM7SF3 drived macrophage M2 polarization by activating the PI3K/AKT /CX3CL1 signaling axis. Trametinib may de as a TM7SF3-targeted drug improved the efficacy of immune checkpoint blockade, and highlighting TM7SF3 as a promising biomarker and therapeutic target for GC.

1.Introduction

Gastric cancer (GC) remains one of the most common malignant tumors of the digestive system and continues to be a leading cause of cancer-related mortality worldwide despite advances in surgical techniques, chemotherapy, targeted therapy, and immunotherapy [1–4]. Although immune checkpoint inhibitors targeting the PD-1/PD-L1 axis have significantly improved the clinical outcomes of selected patients with advanced GC, only a subset of patients achieves durable responses, and both primary and acquired resistance remain major clinical challenges, highlighting the urgent need to identify additional regulators that shape the tumor immune microenvironment[5–7]. Increasing evidence indicates that therapeutic resistance is not solely determined by the intrinsic molecular characteristics of tumor cells but is also profoundly influenced by the tumor immune microenvironment (TIME), where dynamic interactions between malignant cells and immune stromal components critically regulate tumor progression, metastasis, and therapeutic responsiveness[8]. Consequently, identifying tumor-intrinsic regulators that remodel the immune microenvironment may provide new therapeutic opportunities for improving immunotherapy efficacy in GC.

Among the diverse immune cell populations within the TIME, tumor-associated macrophages (TAMs) represent one of the most abundant and functionally important components[9–12]. Depending on environmental cues, macrophages undergo polarization toward either classically activated M1 macrophages with antitumor properties or alternatively activated M2 macrophages that promote tumor growth, angiogenesis, extracellular matrix remodeling, immune suppression, and resistance to systemic therapies [13–14]. In GC, abundant infiltration of M2-polarized TAMs is consistently associated with advanced tumor stage, lymph node metastasis, poor prognosis, and reduced responses to immunotherapy[15]. Accordingly, therapeutic strategies aimed at limiting macrophage recruitment or reprogramming M2 macrophages toward an antitumor phenotype have emerged as promising approaches for remodeling the immunosuppressive microenvironment.

Chemokine-mediated communication between tumor cells and macrophages is increasingly recognized as a key mechanism governing immune-cell recruitment and functional polarization[16]. Among these chemokines, CX3CL1 (fractalkine) is unique because it exists in both membrane-bound and soluble forms, enabling it to regulate immune-cell adhesion, migration, and intercellular communication through its cognate receptor CX3CR1[17]. Dysregulation of the CX3CL1/CX3CR1 axis has been implicated in tumor progression, metastatic dissemination, angiogenesis, and immune escape across multiple solid tumors[18–19]. Emerging evidence further suggests that CX3CL1 participates in macrophage recruitment and polarization, thereby contributing to the establishment of an immunosuppressive tumor microenvironment[20–21]. However, the upstream molecular mechanisms controlling CX3CL1 expression in GC remain incompletely understood. Meanwhile, activation of the PI3K/AKT signaling pathway is one of the most frequently observed oncogenic events in GC and regulates multiple malignant phenotypes, including cell proliferation, survival, apoptosis resistance, migration, metabolic reprogramming, and immune evasion[22–24]. Recent studies have also demonstrated that aberrant PI3K/AKT signaling contributes to macrophage polarization and chemokine production, suggesting a potential mechanistic link between intracellular oncogenic signaling and immune remodeling[25–26].

Transmembrane 7 superfamily member 3 (TM7SF3) is an evolutionarily conserved seven-transmembrane protein that has recently attracted attention because of its role in maintaining endoplasmic reticulum homeostasis, suppressing cellular stress responses, and protecting cells from apoptosis[27]. Although TM7SF3 has been implicated in cell survival under physiological and pathological stress conditions, its biological function in human malignancies remains largely unexplored[28–29]. More importantly, whether TM7SF3 regulates tumor immunity or participates in macrophage-mediated immune remodeling has not been investigated. Based on our preliminary transcriptomic analyses and bioinformatic observations, we found that TM7SF3 expression was markedly elevated in GC and strongly correlated with macrophage infiltration, suggesting that TM7SF3 may exert tumor-promoting effects beyond its previously reported anti-apoptotic function.

Here, we identified TM7SF3 as a previously unrecognized regulator of GC immune remodeling. Through integrated transcriptomic analysis, functional assays, and in vivo models, we demonstrated that TM7SF3 activates PI3K/AKT signaling to enhance CX3CL1 secretion, thereby promoting M2 macrophage polarization and immune escape. Furthermore, we showed that pharmacological targeting of this axis improves the therapeutic efficacy of PD-1 blockade.

2.Methods

2.1 Public datasets and bioinformatic analyses

Gene expression profiles and corresponding clinicopathological information for GC (GC) were obtained from The Cancer Genome Atlas stomach adenocarcinoma (TCGA-STAD) cohort and Gene Expression Omnibus (GEO) datasets. TM7SF3 expression across different human cancers was analyzed using the TIMER2.0 database. Differential expression of TM7SF3 according to tumor stage, histological grade and lymph node status was evaluated using the UALCAN platform.The prognostic significance of TM7SF3 was assessed using the Kaplan–Meier Plotter and PrognoScan databases. Overall survival (OS) was compared between patients with high and low TM7SF3 expression using the optimal cutoff automatically generated by each database.

To investigate the relationship between TM7SF3 and the tumor immune microenvironment, immune-cell infiltration was analyzed using TIMER2.0 and GEPIA2. Correlations between TM7SF3 expression and immune-cell marker genes were evaluated using Spearman's correlation analysis after adjustment for tumor purity where applicable.Single-cell RNA sequencing analysis was performed using the GSE134520 dataset obtained from the scTIME Portal to determine the cellular distribution of TM7SF3 within the GC microenvironment.

Potential therapeutic agents associated with TM7SF3 expression were screened using the Cancer Therapeutics Response Portal (CTRP) and the Cancer Cell Line Encyclopedia (CCLE). Drug sensitivity was evaluated according to the half-maximal inhibitory concentration (IC50), and the correlation between TM7SF3 expression and IC50 values was analyzed using Spearman correlation.

2.2 Tissue specimens

Primary GC tissues and matched adjacent non-tumorous gastric tissues were collected from patients at Nanfang Hospital, Southern Medical University. None of the patients had received chemotherapy, radiotherapy or immunotherapy before surgery. Tissue samples were immediately frozen in liquid nitrogen after surgical resection and stored at − 80°C until RNA and protein extraction. For immunohistochemical analysis, paired paraffin-embedded specimens were collected from the same patient cohort. Histopathological diagnosis was independently confirmed by two experienced pathologists. This study was approved by the Institutional Ethics Committee of Nanfang Hospital, Southern Medical University, and written informed consent was obtained from all participants in accordance with the Declaration of Helsinki.

2.3 Cell culture

Human GC cell lines AGS, MKN-45,SNU-216, NCI-N87, SGC-7901, HGC-27, SNU-1 and the murine GC cell line MFC, and the immortalized human gastric epithelial cell line GES-1 were maintained in RPMI-1640 medium supplemented with 10% fetal bovine serum (FBS) and 1% penicillin–streptomycin at 37°C in a humidified incubator containing 5% CO_2.THP-1 were cultured in RPMI-1640 medium (Gibco) supplemented with 10% FBS. Bone marrow-derived macrophages (BMDMs) were isolated from 6–8-week-old mice and differentiated using L929 cell-conditioned medium as described below.Stable TM7SF3-overexpressing and TM7SF3-knockdown cell lines were established using lentiviral vectors from Jiyuan Biosciences, Guangzhou, China. Cells transduced with empty vectors or scramble shRNA served as negative controls.

2.4 Quantitative real-time PCR

Total RNA was extracted using TRIzol reagent (Invitrogen, USA) according to the manufacturer's instructions. Complementary DNA (cDNA) was synthesized using a reverse transcription kit (Vazyme, China). Quantitative real-time PCR (qRT-PCR) was performed using ChamQ Universal SYBR qPCR Master Mix (Vazyme) on a QuantStudio 6 Flex Real-Time PCR System (Applied Biosystems).Relative gene expression was calculated using the 2^−ΔΔCt method with GAPDH as the endogenous reference gene. Primer sequences are listed in Supplementary Table S1.

2.5 Western blotting

Total cellular proteins were extracted using RIPA lysis buffer supplemented with protease and phosphatase inhibitors. Protein concentration was determined using a bicinchoninic acid (BCA) assay. Equal amounts of protein were separated by SDS-PAGE and transferred onto polyvinylidene fluoride (PVDF) membranes. After blocking with 5% non-fat milk for 1 h at room temperature, membranes were incubated overnight at 4°C with primary antibodies against TM7SF3, AKT, phospho-AKT (Ser473), mTOR, phospho-mTOR (Ser2448), CX3CL1 and β-actin (Proteintech, China). Following incubation with HRP-conjugated secondary antibodies, immunoreactive bands were visualized using enhanced

chemiluminescence (ECL) reagents and quantified using ImageJ software. β-actin served as the loading control.

2.6 Immunohistochemistry (IHC)

Paraffin-embedded GC tissues and corresponding xenograft tumor tissues were sectioned at 4 μm thickness. Following deparaffinization in xylene and rehydration through graded ethanol, antigen retrieval was performed by heating the sections in citrate buffer (pH 6.0). Endogenous peroxidase activity was blocked with 3% hydrogen peroxide for 15 min, followed by blocking with 5% bovine serum albumin for 30 min at room temperature.Sections were incubated overnight at 4°C with primary antibodies against TM7SF3, CX3CL1, CD68, CD86 and CD163 (Proteintech, China). After washing with phosphate-buffered saline (PBS), sections were incubated with HRP-conjugated secondary antibodies for 1 h at room temperature. Immunoreactivity was visualized using 3,3'-diaminobenzidine (DAB), followed by hematoxylin counterstaining. Staining intensity and the percentage of positive cells were independently evaluated by two experienced pathologists blinded to the clinicopathological information. The immunoreactive score (IRS) was calculated by multiplying staining intensity by the percentage of positive cells.

2.7 RNA sequencing and gene set enrichment analysis

Total RNA was extracted from TM7SF3-overexpressing and corresponding control GC cells using TRIzol reagent. RNA quality was evaluated using an Agilent 2100 Bioanalyzer prior to library construction.RNA sequencing libraries were prepared according to the manufacturer's instructions and sequenced on the Illumina NovaSeq 6000 platform. Differentially expressed genes (DEGs) were identified using DESeq2 with an adjusted P value < 0.05 and $|\log_2$ fold change| > 1.Kyoto Encyclopedia of Genes and Genomes (KEGG) pathway enrichment and Gene Ontology (GO) analyses were performed using the clusterProfiler R package. Gene Set Enrichment Analysis (GSEA, version 4.3.2) was further conducted to identify significantly enriched biological pathways. Hallmark and KEGG gene sets downloaded from the Molecular Signatures Database (MSigDB) were used as reference datasets. Gene sets with a false discovery rate (FDR) < 0.25 and nominal P < 0.05 were considered significantly enriched.

2.8 Preparation of conditioned medium and macrophage polarization assay

Human THP-1 monocytes were differentiated into M0 macrophages by treatment with 100 ng/mL phorbol 12-myristate 13-acetate (PMA) for 24 h, followed by incubation in fresh medium for an additional 24 h. Conditioned medium (CM) was collected from TM7SF3-overexpressing, TM7SF3-knockdown and corresponding control GC cells cultured in serum-free medium for 48 h. Cell debris was removed by centrifugation and the supernatant was filtered through a 0.22-μm membrane. M0 macrophages or murine bone marrow-derived macrophages (BMDMs) were cultured with conditioned medium supplemented with 10% FBS for 48 h. Macrophage polarization was subsequently evaluated by quantitative PCR and flow cytometry.

2.9 Enzyme-linked immunosorbent assay (ELISA)

CX3CL1 concentrations in conditioned media were quantified using a commercially available human(KE00145, Proteintech, China) and mouse(SH33177, ZOKEYO, China) CX3CL1 ELISA kit according to the manufacturer's protocol. Briefly, conditioned media were collected after 24 h of serum-free culture and centrifuged to remove cellular debris. Absorbance was measured at 450 nm using a microplate reader. CX3CL1 concentrations were calculated from standard curves generated using recombinant CX3CL1 protein.

2.10 Flow cytometry

Apoptosis of GC cells was evaluated using an Annexin V-APC/Propidium Iodide apoptosis detection kit according to the manufacturer's instructions. After staining, samples were analyzed using a CytoFLEX flow cytometer (Beckman Coulter).

For macrophage polarization analysis, single-cell suspensions isolated from tumors or cultured macrophages were incubated with Fc receptor blocking reagent before staining with fluorochrome-conjugated antibodies against CD45, F4/80, CD86 and CD206. Dead cells were excluded using a viability dye. Data were analyzed using FlowJo software (version 10.8). Macrophages were identified as $CD45^+F4/80^+$ cells, while M1-like and M2-like macrophages were defined as $CD45^+F4/80^+CD86^+$ and $CD45^+F4/80^+CD206^+$ populations, respectively.

2.11 Murine tumor model and therapeutic treatment

Female 615 mice (6–8 weeks old) were purchased from an accredited animal facility and maintained under specific pathogen-free conditions.MFC cells stably overexpressing Tm7sf3 or control cells were subcutaneously injected into the right flank of each mouse (1×10^6 cells per mouse). Tumor volume was measured every three days using calipers and calculated as:

Tumor volume = $(\text{length} \times \text{width}^2)/2$.

When tumors reached approximately 80–100 mm^3, mice were randomly assigned to receive anti-PD-1 monoclonal antibody (5 mg/kg, intraperitoneally, twice weekly), or Trametinib (1 mg/kg, intraperitoneally, twice weekly) with anti-PD-1 monoclonal antibody (5 mg/kg, intraperitoneally, twice weekly) combination therapy.At the end of treatment, tumors were excised, weighed and processed for flow cytometry and immunohistochemistry.

All animal experiments were approved by the Institutional Animal Care and Use Committee of Southern Medical University and were conducted in accordance with institutional guidelines.

2.12 Patient-derived organoid culture and drug sensitivity assay

Fresh GC tissues were obtained immediately after surgical resection and mechanically dissociated into small fragments. Tissue samples were enzymatically digested to obtain single cells, which were embedded in growth factor-reduced Matrigel and cultured in human gastric organoid medium. Organoids were passaged every 7–10 days. Cell proliferation was evaluated using EdU staining.

For drug sensitivity assays, organoids were seeded in 96-well plates and treated with serial concentrations of Trametinib for 5–7 days. Cell viability was determined using the CellTiter-Glo® 3D Cell Viability Assay (Promega). Dose–response curves and half-maximal inhibitory concentrations (IC50) were calculated using GraphPad Prism.

2.13 Extraction of murine bone marrow-derived macrophages

6–8 weeks 615 mice were taken off the cervical vertebrae and executed, soaked in 75% ethanol. The skin of the legs was cut with scissors, and the muscles around each leg bone were thoroughly stripped. Trying not to destroy the integrity of the joint, and each leg bone was placed in 75% alcohol soak and then soak in PBS. Cut the ends of the leg bones and rinse out the cells in the bone marrow by aspirating DMEM medium with a syringe. Discard supernatant, add erythrocyte lysate and gently resuspend for about 2 minutes, followed by DMEM medium with 3–5 times the volume of lysate to terminate lysis. 300g, centrifuge for 5 minutes. Resuspend cells with DMEM containing 20% L929 CM, count and spread in 6-well plates. The medium was changed once every 3 days. Generally, BMDM can be induced to mature after 6 days of culture.

2.14 Statistical analysis

Statistical analyses were performed using GraphPad Prism (version 10.0) and R software (version 4.3.1).Data are presented as the mean ± standard deviation (SD) from at least three independent experiments. Differences between two groups were analyzed using unpaired two-tailed Student's t-test, whereas comparisons among multiple groups were performed using one-way ANOVA followed by Tukey's multiple comparison test. Correlations between gene expression levels were evaluated using Spearman's correlation coefficient. Overall survival was estimated using the Kaplan–Meier method and compared using the log-rank test. Cox proportional hazards regression analysis was performed to identify independent prognostic factors where appropriate. A two-sided P value < 0.05 was considered statistically significant.

3.Results

3.1 TM7SF3 is upregulated in GC and predicts poor prognosis

To analyze TM7SF3 expression in different cancers, TM7SF3 mRNA expression was analyzed in The Cancer Genome Atlas (TCGA)-Pan-Cancer datasets by using the TIMER database. As shown in Fig. 1A,

the results indicated that TM7SF3 mRNA expression was markedly elevated in the tumor tissues of cholangiocarcinoma (CHOL), esophageal carcinoma (ESCA), head and neck squamous cell carcinoma (HNSC), liver hepatocellular carcinoma (LIHC), lung squamous carcinoma (LUSC), stomach adenocarcinoma (STAD), and thyroid carcinoma (THCA) when compared to their corresponding normal tissues in cancers. Conversely, TM7SF3 mRNA expression was significantly reduced in the kidney chromophobe (KICH), prostate adenocarcinoma (PRAD), kidney renal clear cell carcinoma (KIRC), and rectum adenocarcinoma (READ) tumor tissues. Additionally, TM7SF3 expression was analyzed in GC tumor tissues from a TCGA-STAD dataset by using the UALCAN database. The results showed that TM7SF3 mRNA expression is significantly associated with the primary tumors, tumor stages, tumor grade, and lymph node metastasis status of GC tumor tissues. Multiple datasets of GC patients from the GEO datasets were further validated that TM7SF3 mRNA expression was significantly upregulated in GC tumor tissues compared to adjacent normal tissues. Furthermore, TM7SF3 mRNA expression levels in the tumor tissues exhibited distinct differences when compared to those in gastritis, low-grade intraepithelial neoplasia, and high-grade intraepithelial neoplasia tissues (Fig. 1B). In the a forementioned findings, we confirmed that TM7SF3 was highly expressed in both tumor tissues and cell lines and is associated with the tumor staging of GC by multiple databases.

We further investigated whether TM7SF3 expression is associated with the prognosis of GC patients. Firstly, we analyzed the survival prognosis of cancer patients with TM7SF3 expression by the PrognoScan database, found that high mRNA expression of TM7SF3 was significantly associated with the poor overall survival (OS) times in the patients with blood cancer (P = 0.0079), brain cancer (P = 0.0044), colorectal cancer (P = 0.0155), pancreatic cancer (P = 0.010), cervical squamous cell carcinoma (P = 0.047) and sarcoma (P = 0.018) respectively based on the GEO and TCGA datasets (Fig. 1C). Moreover, we analyzed three GC-patient cohorts in GEO datasets and found that high TM7SF3 expression was significantly associated with poor OS times of GC patients from GSE15459 (P = 0.036) and GSE14210 (P = 0.028) respectively (Fig. 1D). We used the Kaplan-Meier plotter database for multivariate Cox proportional hazards modeling in the GSE15459 and GSE14210, found that TM7SF3 expression as an independent predictor of survival for GC patients with T3 stage (HR = 2.02, P = 0.0057) and poorly differentiation (HR = 1.76, P = 0.026) in the GSE15459, and for GC patients with positive HER2 status (HR = 1.87, P = 0.021) and 5-FU based adjuvant treatment (HR = 1.56, P = 0.028) in the GSE14210 (Table.2). Collectively, these findings suggested that high TM7SF3 expression predict poor prognosis of GC patients, TM7SF3 is acted as a novel prognostic biomarker for GC patients.

3.2 TM7SF3 promotes the malignant phenotype of GC cells

we evaluated the expression levels of TM7SF3 in GES-1 (human normal gastric mucosal cell line) and other GC cell lines. Then, we observed that TM7SF3 mRNA and protein levels were elevated in most of the GC cell lines compared to the levels in GES-1 cells (Fig. 2A). We examined mRNA and protein levels of adjacent normal gastric tissues and paired GC tumor tissues by the quantitate real-time PCR and western blotting assays. These results indicated that TM7SF3 mRNA and protein levels were elevated in the tumor tissues compared to paired normal gastric tissues (Fig. 2B). Furthermore,

immunohistochemistry assay results revealed that as the tumor staging of GC progresses, there is a increase in TM7SF3 expression level, implying an association between TM7SF3 expression and the progression of GC (Fig. 2C). To better understand the relationship of TM7SF3 expression and tumor progression in GC, we investigated the clinical characteristics of GC patients with TM7SF3 expression by using the TCGA-STAD dataset, found that these GC patients at the T4 stage exhibited significantly higher TM7SF3 expression levels compared to those patients at T1-3 stages (P = 0.038), suggesting that TM7SF3 mRNA expression is associated with the T stage in the GC patients (Table 1). To investigate the biological function of TM7SF3 in GC, stable TM7SF3-overexpressing (LV-TM7SF3) and TM7SF3-knockdown (sh-TM7SF3-1 and sh-TM7SF3-2) MKN-45, AGS cell lines, together with their corresponding negative controls (LV-NC and shNC), were established using one overexpression lentiviral vector and two independent shRNA lentiviral vectors. We also generated MFC cells with Tm7sf3 overexpression and knockdown lentiviral vectors (Figure S1B). Cell migration was evaluated by wound-healing assays, and the wound closure rate was quantified (Fig. 2D&Figure S1C). In addition, transwell migration and colony formation assays also indicated that TM7SF3 promoted proliferation and migaration of GC cells (Fig. 2E&Figure S1C). Given the reported anti-apoptotic role of TM7SF3 in maintaining cellular homeostasis, we next investigated whether TM7SF3 regulates apoptosis in GC cells. TM7SF3 overexpression significantly decreased the proportion of apoptotic cells, whereas TM7SF3 knockdown enhanced apoptosis (Fig. 2F). These findings demonstrate that TM7SF3 expression level was elevated in both GC tumor tissues and cell lines, and it may be positively associated with the progression of gastric caner.

3.3 TM7SF3 expression is associated with macrophage infiltration

To reveal the correlation between TM7SF3 expression and immune cells in GC microenvironment, a comprehensive analysis of TM7SF3 expression and immune cell in TCGA-STAD dataset revealed that the proportions of immune cell populations differ between tumor and normal tissues in GC, with significant differences in these various immune cells including the plasma cells, naïve B cells, CD4 memory resting T cells, CD4 memory activated T cells, follicular helper T cells, regulatory Tregs T cells, activated mast cells, resting NK cells, M0, M1 and M2 macrophages (Figure.3A). Moreover, we observed that up-regulation of TM7SF3 expression in various cell types within the tumor tissues, including naïve B cells, CD4 memory resting T cells, CD4 memory activated T cells, follicular helper T cells, regulatory Tregs T cells, resting NK cells, and M0, M1, and M2 macrophages, when compared to their expression levels in the corresponding normal tissues. Interestingly, the differences of TM7SF3 expression associated with M0, M1, and M2 macrophages were the most significant (***, P-value < 0.001) (Fig. 3B). Meanwhile, a GC-related scRNA-seq dataset GSE134520 from scTIME database was used to analyze the expression level of TM7SF3 at the single-cell level (Fig. 3C). These single-cell data were showed the cell clusters and types in the GC tumor microenvironment. After the cluster analysis of various cell types, the results found that the abundance of TM7SF3 was mainly enriched in cancer cells of early GC (EGC) tissues (Fig. 3D), suggesting that TM7SF3 was highly expressed in the tumor cells of GC. Considering the association with tumor-infiltrating immune cells in TME, we analyzed the corrections between TM7SF3

and gene markers of immune cells in TCGA-STAD dataset. We found that TM7SF3 mRNA expression correlated with the expression levels of these gene markers of CD4 + T cell, CD8 + T cell, T cell exhaustion, monocyte, neutrophils, TAM, M1 Macrophage, M2 Macrophage, NK cell, dendritic cell, T helper cell, follicular helper T cell and regulatory Tregs T cells in the GC microenvironment (Table 3). These results indicated that TM7SF3 expression was relative to the infiltration of immune cells in the GC microenvironment.

3.4 TM7SF3 drives macrophage M2 polarization in vitro and in vivo

Given previous results have found that TM7SF3 correlated to the infiltration of immune cells in the tumor microenvironment (TME), macrophages were considered as the most significant immune cell population associated with TM7SF3 expression, consistent with the concept that tumor-intrinsic signaling profoundly shapes immune-cell infiltration and antitumor immunity[30–32].We further analyzed the relationship between TM7SF3 expression and macrophages. Based on the survival analysis of diverse types of immune cells on the TCGA-STAD dataset, the results revealed that GC patients with high infiltration of macrophage have poor survival prognosis (HR = 1.27, *P* = 0.002), as well as these GC patients with high infiltration of macrophage and high TM7SF3 expression have poor survival prognosis (HR = 2.36, *P* = 0.0006) (Fig. 4A). Simultaneously, these GC patients exhibiting high infiltration of M2 macrophages and high TM7SF3 expression have poor survival times (HR = 2.01, *P* = 0.0055) (Fig. 4B). Besides the infiltration of M2 macrophages, the infiltration of other immune cell types did not show a significant correlation with patient outcomes. (Figure S1). By using the TIMER-STAD database, we found that TM7SF3 expression was associated with the infiltration levels of macrophage and M2 macrophages, as well as the expression of CD68 and CD163 positively (Fig. 4C). Immunohistochemical assays also validated the correlation of expressing infiltrations among macrophage, M1 macrophages and M2 macrophages in GC tumor tissues by the staining of TM7SF3, CD68, CD86 and CD163, indicating that high expression level of TM7SF3 was significantly associated with high infiltrations of macrophage and M2 macrophages, and low infiltration of M1 macrophages (Fig. 4D). We performed the Gene Set Enrichment Analysis (GSEA) software to analyze the potential mechanism of TM7SF3 and macrophage. The GC patients from GEO datasets were averagely divided into two groups according to the expression level of TM7SF3. The results from an enrichment analysis declared that a Gene Ontology (GO) biological process of macrophage-activation involved in the immune response was significantly enriched in the TM7SF3 high expression group (Fig. 4E). By enrichment analysis between the GC tumor tissues and paired normal tissues in GEO datasets, the biological process of macrophage-activation involved in the immune response was shown to be enriched in the GC tumor tissue (Figure S2). The correlation between TM7SF3 mRNA expression and the key genes of macrophage activation, recruitment and polarization were analyzed in the TCGA-STAD dataset (Supplementary Table 2 & Supplementary Table 3). To mimic tumor–macrophage interactions, conditioned media derived from TM7SF3-overexpressing or TM7SF3-knockdown GC cells were collected and applied to PMA-induced THP-1-derived macrophages (Fig. 4F). Quantitative PCR analysis revealed that conditioned medium from TM7SF3-overexpressing cells significantly increased the expression of the M2-associated markers CD163 and TGFB1, whereas the

expression of the M1-associated markers CD86 and TNF was markedly reduced (Fig. 4H). Conversely, conditioned medium from TM7SF3-knockdown cells produced the opposite effect, indicating that tumor-derived TM7SF3 favors macrophage polarization toward an M2 phenotype. To further validate these findings under physiological conditions, murine bone marrow-derived macrophages (BMDMs) were cultured with conditioned medium derived from MFC cells. Similar to the observations in THP-1-derived macrophages, TM7SF3 overexpression significantly upregulated the M2 markers Fizz1 and Mgl2, while suppressing the expression of the classical M1 markers Nos2 and Tnf (Fig. 4G&Figure 4I). These results suggest that TM7SF3-mediated macrophage polarization is conserved across both human and murine macrophage models.

Phenotypic alterations in macrophages were further quantified by flow cytometry. Exposure to conditioned medium from Tm7sf3-overexpressing MFC cells significantly increased the proportion of $F4/80^{+}CD206^{+}$ M2-like macrophages, accompanied by a marked reduction in $F4/80^{+}CD86^{+}$ M1-like macrophages (Fig. 5A). In contrast, conditioned medium from TM7SF3-knockdown cells reversed this polarization pattern, further confirming that TM7SF3 promotes macrophage polarization toward an immunosuppressive phenotype. To determine whether these observations could be recapitulated in vivo, subcutaneous tumor models were established by inoculating Tm7sf3-overexpressing, Tm7sf3-knockdown and control MFC cells into 615 mice. Tumors derived from Tm7sf3-overexpressing cells exhibited significantly accelerated growth compared with control tumors (Fig. 5B), indicating that TM7SF3 enhances tumor progression in vivo. Immunohistochemical staining revealed stronger TM7SF3 expression accompanied by increased CD206-positive macrophage infiltration within Tm7sf3-overexpressing tumors (Fig. 5C). Consistent with these findings, flow cytometric analysis of tumor-infiltrating immune cells further demonstrated that tumors with elevated Tm7sf3 expression contained a significantly higher proportion of CD206-positive M2 macrophages and a reduced proportion of CD86-positive M1 macrophages (Fig. 5D). These data demonstrate that TM7SF3 actively reprograms macrophage polarization toward an M2-like phenotype both in vitro and in vivo, thereby establishing an immunosuppressive tumor microenvironment that is favorable for GC progression.

3.5 TM7SF3 activates PI3K/AKT signaling to induce CX3CL1 secretion and promote macrophage M2 polarization

Hence, these findings suggested that TM7SF3 was positively associated with the function of macrophage for the tumor immune response in GC. It is known that tumor-infiltrating macrophage are recruited, activated and polarized into M1 or M2 macrophages in the TME. M2 macrophages are usually deemed as tumor-associated macrophages (TAMs), contribute to the pro-tumorigenic outcomes in cancer. The interaction of TM7SF3 and the infiltration of M2 macrophages is involved in the process of activation, recruitment and polarization on macrophage. The results from a Venn diagram showed that CX3CR1 was a key hub-gene of the recruitment, activation, polarization of macrophage by the gene sets analysis (Fig. 6A). CX3CR1 binds to its ligand CX3CL1, CX3CR1-CX3CL1 axis participates in the process of recruitment, activation and polarization of macrophage. We analyzed the TCGA-STAD database to

reveal the associations among TM7SF3, CX3CR1 and CX3CL1 at mRNA expression level, found the correlations between any two of them significantly in GC (Fig. 6B).

Because chemokine-mediated communication plays a central role in macrophage recruitment and polarization, we next examined whether TM7SF3 regulates the expression of CX3CL1. qRT-PCR and ELISA consistently demonstrated that TM7SF3 overexpression significantly increased both intracellular expression and extracellular secretion of CX3CL1, whereas TM7SF3 depletion markedly reduced CX3CL1 production (Fig. 6C-D). Given the previously mentioned relationship between CX3CL1 and CX3CR1, we examined CX3CR1 expression in THP-1 and BMDMs cultured with supernatants from MKN-45, AGS, and MFC cells; the results showed that high expression of TM7SF3 can also lead to high expression of CX3CR1 in THP-1 cells and BMDMs (Fig. 6E). IHC staining of GC tissues revealed that tumors with high TM7SF3 expression also exhibited stronger CX3CL1 staining than TM7SF3-low tissues. Correlation analysis further demonstrated a significant positive association between TM7SF3 and CX3CL1 protein expression ($R^2 = 0.318$, $P < 0.0001$) (Fig. 6F). RNA-seq analysis identified several significantly enriched signaling pathways following TM7SF3 overexpression, including the p53 and PI3K/AKT pathways (Figure S5A). Given that previous studies have established TM7SF3 as a p53-regulated homeostatic factor involved in cellular stress responses and apoptosis [27], we focused our subsequent mechanistic investigation on the PI3K/AKT pathway, for which the potential role in TM7SF3-mediated tumor–macrophage communication has not been established. Notably, PI3K/AKT signaling is closely associated with tumor-cell survival and macrophage polarization. Consistent with the transcriptomic analysis, Western blotting demonstrated increased activation of the PI3K/AKT pathway following TM7SF3 overexpression (Fig. 6G). To determine whether PI3K/AKT signaling mediates TM7SF3-induced CX3CL1 expression, pharmacological rescue experiments were performed[33–34]. We assessed CX3CL1 expression using qRT-PCR and demonstrated that the blockade of the PI3K-AKT pathway by MK2206 (10 μM) led to the downregulation of CX3CL1 expression, whereas SC79 (10 μM) restored CX3CL1 expression(Figure S5B). Flow cytometric analysis of Annexin V/PI staining demonstrated that treatment with the AKT inhibitor MK2206 significantly increased apoptosis in TM7SF3-overexpressing GC cells, whereas subsequent treatment with the AKT activator SC79 partially rescued this effect, indicating that AKT signaling mediates the anti-apoptotic function of TM7SF3 (Fig. 6H). Moreover, flow cytometry further showed that conditioned medium derived from TM7SF3-overexpressing cells significantly increased the proportion of $CD206^+$ M2 macrophages and reduced $CD86^+$ M1 macrophages. MK2206 reversed TM7SF3-induced macrophage M2 polarization, whereas SC79 partially restored this phenotype, indicating that TM7SF3 promotes macrophage M2 polarization through activation of the PI3K/AKT pathway (Fig. 6I). We also used qRT-PCR to detect M1 and M2 markers (Figure S5C-D). In a word, these results demonstrate that TM7SF3 activates the PI3K/AKT signaling pathway to upregulate CX3CL1 expression, thereby promoting CX3CR1-dependent macrophage M2 polarization and contributing to an immunosuppressive tumor microenvironment in GC.

3.6 Trametinib is identified as potential drug depending on TM7SF3 expression

Considering our previous findings, TM7SF3 might be a potential target for GC treatment. We further analyzed the mRNA and protein expression of TM7SF3 in the different GC cell lines by using the CCLE database. We identified that several GC cell lines as TM7SF3-high cells, including AGS, MKN-45, OCUM1, MKN1, and KATO III. While other GC cell lines were classified as TM7SF3-low cells, such as MKN-7, HGC-27, SNU-1, IM95, and NCI-N87 (Figure S6A). To identify potential therapeutic drugs based on the expression level of TM7SF3, we analyzed the IC50 (50% inhibitory concentration) values of candidate drugs through using the CTRP database. A volcano plot was used to screen the differential drugs between the TM7SF3-high cells and TM7SF3-low cells, the IC50 values of thirteen candidate drugs including KIN001-244, Quizartinib, TL-1-85, OSI-027, Linaltinib, Masitinib, XMD14-99, KIN001-236, THZ-2-49, TL-2-105, and Trametinib, exhibited significant differences when comparing the TM7SF3-high cells with TM7SF3-low cells (Figure S6B). The differential analysis confirmed that KIN001-244, Quizartinib, TL-1-85, OSI-027, Linaltinib, Masitinib, XMD14-99, KIN001-236, THZ-2-49, and TL-2-105 were increased in TM7SF3-high cells, whereas the IC50 value of Trametinib was significantly reduced (Figure S6C). Concurrently, the correlation analysis between the IC50 value of these candidate drugs and TM7SF3 expression in GC cell lines revealed that the IC50 value of Trametinib was negatively correlated with the expression level of TM7SF3 in the GC cell lines (Spearman R = − 0.758, P = 0.015) (Figure S6D). We analyzed the associations between the trametinib and the expression level of TM7SF3, found that these GC cell lines with high TM7SF3 expression demonstrated lower IC50 values compared to those with low TM7SF3 expression (P = 0.028) (Figure S6E). A heatmap showed the dose-response scores of thirteen candidate drugs between the TM7SF3-high cells and TM7SF3-low cells (Figure S6F). A dose-response analysis indicated that these GC cell lines with low TM7SF3 expression demonstrated higher drug response to Trametinib, compared to those with high TM7SF3 expression (Figure S6G).

To evaluate the clinical relevance of TM7SF3, GC patient-derived organoids (PDOs) with high or low TM7SF3 expression were established. IHC confirmed differential TM7SF3 expression in the corresponding patient tissues, which was retained in the derived organoids (Fig. 7A). EdU staining further demonstrated that TM7SF3^{high} PDOs exhibited significantly greater proliferative activity than TM7SF3^{low} PDOs (Fig. 7B). Compared with TM7SF3^{low} organoids, TM7SF3^{high} organoids exhibited significantly greater sensitivity to Trametinib, as reflected by lower IC50 values and more pronounced inhibition of organoid growth with IC50 values of 0.179 μM and 0.219 μM (Fig. 7C-D). Consistently, bright-field imaging revealed a dose-dependent suppression of organoid growth following Trametinib treatment, with a more pronounced inhibitory effect in TM7SF3^{high} PDOs (Fig. 7E). Finally, in vivo experiments demonstrated that TM7SF3 overexpression reduced the antitumor efficacy of anti-PD-1 therapy. Importantly, combination treatment with Trametinib (1 mg/kg) and anti-PD-1 mAb (5 mg/kg) markedly inhibited tumor growth and decreased tumor weight compared with anti-PD-1 monotherapy, indicating that Trametinib effectively enhanced immunotherapeutic efficacy (Fig. 7F). Given the above, these findings indicate that TM7SF3 promotes PDO growth and confers resistance to anti-PD-1 therapy, whereas Tramtinib effectively suppresses TM7SF3-driven tumor progression and sensitizes GC to immune checkpoint blockade.

4.Discussion

GC remains a highly heterogeneous malignancy in which aberrant oncogenic signaling and immune dysregulation cooperatively drive tumor progression and therapeutic resistance[35]. Although immune checkpoint inhibitors have improved the prognosis of a subset of patients with advanced GC, the majority fail to achieve durable clinical benefit because of an immunosuppressive tumor microenvironment. Therefore, elucidating the molecular mechanisms by which tumor cells reshape immune-cell function is essential for identifying predictive biomarkers and developing more effective therapeutic strategies. In the present study, we identified TM7SF3 as a previously unrecognized regulator of macrophage-mediated immune remodeling in GC. By integrating bioinformatic analyses, clinical validation, in vitro functional assays, transcriptomic profiling, mechanistic studies, patient-derived organoids, and syngeneic mouse models, we demonstrated that TM7SF3 promotes GC progression by activating PI3K/AKT signaling, enhancing CX3CL1 expression and secretion, inducing macrophage M2 polarization, and establishing an immunosuppressive tumor microenvironment. Furthermore, pharmacological inhibition using Trametinib restored antitumor immunity and significantly improved the therapeutic efficacy of anti-PD-1 treatment. These findings identify a previously unrecognized TM7SF3–PI3K/AKT–CX3CL1 signaling axis that links tumor-intrinsic signaling to immune microenvironment remodeling.

Previous study has reported that TM7SF3 is considered as a p53-regulated homeostatic factor that can attenuate cellular stress and unfolded protein response (UPR)[27]. Overexpression of TM7SF3 inhibits caspase 3/7 activation, reduces the apoptosis in human islets and MIN6 cells. Conversely, silencing TM7SF3 accelerates endoplasmic reticulum (ER) stress and induces apoptosis through the UPR pathway[36]. TM7SF3 plays a crucial role in regulating ER stress by inhibiting key pro-apoptotic factors such as CHOP, ATF3, and ATF4[37]. High levels of TM7SF3 may maintain protein homeostasis and promote tumor cell survival by alleviating endoplasmic reticulum (ER) stress. Additionally, TM7SF3 is found to be involved in the pathogenesis of rat breast cancer, and it may also be involved in the process of sulindac treatment for colon cancer[38]. However, its function in human malignancies remains poorly understood. Previous studies primarily focused on the cytoprotective role of TM7SF3 under physiological conditions, whereas its contribution to tumor progression and immune regulation has received little attention. Our data extend the biological function of TM7SF3 beyond its established anti-apoptotic activity by demonstrating that TM7SF3 enhances GC cell proliferation and migration while protecting tumor cells from apoptosis. More importantly, we show that TM7SF3 exerts profound effects on the tumor microenvironment, indicating that its oncogenic activity is mediated not only through direct regulation of tumor-cell behavior but also through modulation of tumor–immune interactions. This dual function may explain why elevated TM7SF3 expression is consistently associated with advanced disease and poor prognosis in patients with GC.

One of the most important findings of this study is the identification of PI3K/AKT signaling as the principal downstream pathway responsible for TM7SF3-mediated immune remodeling. Aberrant activation of PI3K/AKT is among the most common oncogenic events in GC and regulates cell

proliferation, survival, metabolism, migration, and therapeutic resistance[39]. Increasing evidence also indicates that PI3K/AKT signaling participates in immune escape by regulating cytokine production, macrophage polarization, and T-cell dysfunction[40–41]. Consistent with these observations, our transcriptomic analysis identified significant enrichment of PI3K/AKT signaling following TM7SF3 overexpression, which was further confirmed by increased phosphorylation of PI3K and AKT[42]. Pharmacological inhibition of this pathway effectively abolished TM7SF3-induced CX3CL1 expression and macrophage polarization, whereas AKT activation partially restored these effects. These rescue experiments establish a causal relationship between TM7SF3 and PI3K/AKT activation, rather than a simple correlation, indicating that PI3K/AKT signaling functions as the central molecular bridge connecting TM7SF3 with immune microenvironment remodeling.

Another major contribution of this study is the identification of CX3CL1 as a downstream effector linking oncogenic signaling to macrophage polarization. M2 macrophages, are also called the tumor-associated macrophages (TAMs) in TME[43]. Recently, the key role of TAMs in human cancers has obtained more and more attention[44]. As the main component of immune cells in TME, TAMs facilitate tumor initiation, metastasis, angiogenesis and immunosuppression through the secretion of signaling pathway regulators or inflammatory factors in TME[45]. TAMs display the remarkable plasticity when stimulating by specific TME signals, serving as a crucial viewpoint for researching anti-cancer therapeutic targets in malignancy[46]. The activation, polarization and recruitment of M2 macrophages promotes tumor progression and metastasis in gastric adenocarcinoma, prostate cancer, colorectal cancer, pancreatic cancer and breast cancer[47]. Our study suggested that TM7SF3 may affect the infiltration of M2 macrophage in the GC microenvironment. CX3CR1 is a cell marker of the activation, polarization and recruitment of macrophages[48]. We found a positive correlation between TM7SF3 and CX3CR1 in the TCGA-STAD dataset. CX3CR1 may be as a potential molecular target on M2 macrophages in TME. CX3CR1 is broadly expressed in the stromal immune cells, including the monocytes, dendritic cells, macrophages, natural killer (NK) cells, T cells. Activation of macrophage-expressing CX3CR1 induces signaling events and cell infiltration in TME. CX3CR1 binds to its ligand CX3CL1, participating in the biological process of activation, polarization and recruitment of macrophage. CX3CL1 is a transmembrane protein that shed into a soluble form through proteolysis[49]. The CX3CL1-CX3CR1 axis drive macrophage to anti-cancer immune evasion in cancer, thereby activating signaling pathways and promoting tumor proliferation, migration, invasion, and resistance to cell apoptosis[50]. Overexpression of CX3CR1 is related to the promotion of tumor proliferation and tumor metastasis, leads to poor prognosis for GC patients. But adequate expression levels of CX3CR1 in the normal gastric tissues might facilitate cell renewal or tissue remodeling post-injury[51]. Our findings demonstrate that TM7SF3-induced activation of PI3K/AKT significantly enhances CX3CL1 expression and secretion, thereby promoting macrophage M2 polarization through paracrine signaling. This mechanism provides a plausible explanation for the strong correlation between TM7SF3 expression and M2 macrophage infiltration observed in both clinical samples and public datasets. Rather than acting as an isolated signaling molecule, CX3CL1 appears to function as a key mediator through which tumor cells communicate with surrounding macrophages to establish an immunosuppressive microenvironment.

These observations broaden the current understanding of CX3CL1 biology in GC and identify TM7SF3 as an upstream regulator of the PI3K/AKT/CX3CL1 axis.

From a translational perspective, our study further demonstrates that targeting TM7SF3-associated signaling may improve the response to immunotherapy. Although PD-1 blockade has become an important therapeutic option for advanced GC, clinical benefit remains limited because of multiple mechanisms of immune escape, including M2 macrophage accumulation[52–53]. Our results indicate that tumors with high TM7SF3 expression exhibit enhanced macrophage-mediated immunosuppression and reduced sensitivity to anti-PD-1 therapy[54–55]. Notably, Trametinib effectively suppressed TM7SF3-driven tumor growth, reduced M2 macrophage infiltration, and significantly potentiated the efficacy of PD-1 blockade in vivo. In addition, patient-derived organoids with high TM7SF3 expression displayed greater sensitivity to Trametinib, suggesting that TM7SF3 may serve not only as a prognostic biomarker but also as a predictive biomarker for therapeutic stratification[56–57]. These findings support the rationale for combining targeted therapy with immune checkpoint blockade in TM7SF3-high GC and provide a potential strategy for overcoming immunotherapy resistance.

Several limitations should be acknowledged. First, although our study demonstrated that TM7SF3 regulates macrophage polarization through the PI3K/AKT/CX3CL1 axis, the transcriptional mechanisms responsible for CX3CL1 upregulation remain to be elucidated. Second, neutralization of CX3CL1 or genetic disruption of CX3CR1 would provide more direct evidence supporting the functional importance of this signaling axis in macrophage polarization. Third, although the therapeutic efficacy of Trametinib was validated using patient-derived organoids and syngeneic mouse models, additional validation in larger clinical cohorts and prospective translational studies will be required before clinical application. Finally, given the complexity of the tumor immune microenvironment, future studies should investigate whether TM7SF3 also influences other immune-cell populations, including cytotoxic T lymphocytes, regulatory T cells, dendritic cells, and cancer-associated fibroblasts.

In conclusion, we demonstrate that TM7SF3 functions as a novel oncogenic regulator in GC by activating the PI3K/AKT signaling pathway and promoting CX3CL1-dependent remodeling of the tumor immune microenvironment (Fig. 8). Through enhancement of M2 macrophage polarization, TM7SF3 contributes to tumor progression and diminished responsiveness to anti-PD-1 immunotherapy. Importantly, pharmacological intervention with trametinib effectively suppresses tumor growth and potentiates immune checkpoint blockade, highlighting the therapeutic potential of targeting TM7SF3 and PI3K-AKT-CX3CL1 axis. All in all, our findings establish TM7SF3 as a promising prognostic biomarker and potential therapeutic target, providing new mechanistic insights and a translational framework for precision immunotherapy in GC.

Declarations

Disclosure

The author(s) report no conflicts of interest in this work.

Data sharing statement

The data supporting the findings of this study are available within the article and/or the supplementary materials.

Acknowledgements and funding sources

This work was supported by these grants awarded to Dr. H.L. by the Natural Science Foundation of Guangdong Province (2023A1515010785), to Dr. Z.Z.Z. by the President Foundation of Nanfang Hospital, Southern Medical University (2025B013), to Dr. G.X.L by the Key Areas Research and Development Programs of Guangdong Province (2023B1111050009).

Author contribution declaration

Z.Z. Zhang were responsible for the study concept and design. H. Liu and Z.Z. Zhang obtained the funding. R. Shen, Q. H. Zheng, Z. Xu, D.H. Huang, J.Y. He and Z.Z. Zhang acquired the data. X.Y. Li, C.X. Mo, Z. Wang helped to collect the data, Z.Z. Zhang and Z.H. Lu analyze and interpret the data. R.Shen, Q.H.Zheng, Z. Xu, D.H. Huang, J.Y. He and Z.Z. Zhang drafted the manuscript, and all authors revised it for important intellectual content.

References

1. Sung H, Ferlay J, Siegel RL, et al. Global cancer statistics 2020: GLOBOCAN estimates of incidence and mortality worldwide for 36 cancers in 185 countries. CA Cancer J Clin. 2021;71:209–249.
2. Hirata Y, Noorani A, Song S, Wang L, Ajani JA. Early stage gastric adenocarcinoma: clinical and molecular landscapes. Nat Rev Clin Oncol. 2023 Jul;20(7):453-469.
3. Smyth EC, Nilsson M, Grabsch HI, et al. GC. Lancet. 2020;396:635–648.
4. Ajani JA, D'Amico TA, Bentrem DJ, Corvera CU, Das P, Enzinger PC, Enzler T, Gerdes H, Gibson MK, Grierson P, Gupta G, Hofstetter WL, Ilson DH, Jalal S, Kim S, Kleinberg LR, Klempner S, Lacy J, Lee B, Licciardi F, Lloyd S, Ly QP, Matsukuma K, McNamara M, Merkow RP, Miller AM, Mukherjee S, Mulcahy MF, Perry KA, Pimiento JM, Reddi DM, Reznik S, Roses RE, Strong VE, Su S, Uboha N, Wainberg ZA, Willett CG, Woo Y, Yoon HH, McMillian NR, Stein M. Gastric Cancer, Version 2.2025, NCCN Clinical Practice Guidelines In Oncology. J Natl Compr Canc Netw. 2025 May;23(5):169-191.
5. Janjigian YY, Al-Batran SE, Wainberg ZA, Muro K, Molena D, Van Cutsem E, Hyung WJ, Wyrwicz L, Oh DY, Omori T, Moehler M, Garrido M, Oliveira SCS, Liberman M, Oliden VC, Smyth EC, Stein A, Bilici M, Alvarenga ML, Kozlov V, Rivera F, Kawazoe A, Serrano O, Heilbron E, Negro A, Kurland JF, Tabernero J; MATTERHORN Investigators. Perioperative Durvalumab in Gastric and Gastroesophageal Junction Cancer. N Engl J Med. 2025 Jul 17;393(3):217-230. Chen DS, Mellman I. Elements of cancer immunity and the cancer-immune set point. Nature. 2017;541:321–330.
6. Binnewies M, Roberts EW, Kersten K, Chan V, Fearon DF, Merad M, Coussens LM, Gabrilovich DI, Ostrand-Rosenberg S, Hedrick CC, Vonderheide RH, Pittet MJ, Jain RK, Zou W, Howcroft TK,

Woodhouse EC, Weinberg RA, Krummel MF. Understanding the tumor immune microenvironment (TIME) for effective therapy. Nat Med. 2018 May;24(5):541-550.

7. Fridman WH, Zitvogel L, Sautès-Fridman C, Kroemer G. The immune contexture in cancer prognosis and treatment. Nat Rev Clin Oncol. 2017 Dec;14(12):717-734.
8. Mantovani A, Marchesi F, Malesci A, Laghi L, Allavena P. Tumour-associated macrophages as treatment targets in oncology. Nat Rev Clin Oncol. 2017 Jul;14(7):399-416.
9. Qian BZ, Pollard JW. Macrophage diversity enhances tumor progression and metastasis. Cell. 2010 Apr 2;141(1):39-51.
10. Yeo EJ, Cassetta L, Qian BZ, Lewkowich I, Li JF, Stefater JA 3rd, Smith AN, Wiechmann LS, Wang Y, Pollard JW, Lang RA. Myeloid WNT7b mediates the angiogenic switch and metastasis in breast cancer. Cancer Res. 2014 Jun 1;74(11):2962-73.
11. Li J, Sun J, Zeng Z, Liu Z, Ma M, Zheng Z, He Y, Kang W. Tumour-associated macrophages in GC: From function and mechanism to application. Clin Transl Med. 2023 Aug;13(8):e1386.
12. Wan C, Deng J, Zhu Y, Wan L, Xu L, Chen Q, Zou C, Huang J. Targeting tumor-associated macrophages in GC progression and therapy: insights from molecular mechanisms to therapeutic applications. Front Pharmacol. 2025 Jun 17;16:1549694.
13. Gong N, Qin G, Sun J, Shen S, Zhang X, Lu M. Therapeutic potential of targeting macrophage polarization in metastatic GC: a review on core mechanisms and clinical progress. Clin Transl Oncol. 2026 Jun 4.
14. DeNardo DG, Ruffell B. Macrophages as regulators of tumour immunity and immunotherapy. Nat Rev Immunol. 2019 Jun;19(6):369-382.
15. Rivas-Fuentes S, Salgado-Aguayo A, Arratia-Quijada J, Gorocica-Rosete P. Regulation and biological functions of the CX3CL1-CX3CR1 axis and its relevance in solid cancer: A mini-review. J Cancer. 2021 Jan 1;12(2):571-583.
16. Lu X. Structure and Function of Ligand CX3CL1 and its Receptor CX3CR1 in Cancer. Curr Med Chem. 2022;29(41):6228-6246.
17. Szukiewicz D. CX3CL1 (Fractalkine)-CX3CR1 Axis in Inflammation-Induced Angiogenesis and Tumorigenesis. Int J Mol Sci. 2024 Apr 25;25(9):4679.
18. Chaudhri A, Bu X, Wang Y, Gomez M, Torchia JA, Hua P, Hung SH, Davies MA, Lizee GA, von Andrian U, Hwu P, Freeman GJ. The CX3CL1-CX3CR1 chemokine axis can contribute to tumor immune evasion and blockade with a novel CX3CR1 monoclonal antibody enhances response to anti-PD-1 immunotherapy. Front Immunol. 2023 Sep 13;14:1237715.
19. Wei LM, Cao S, Yu WD, Liu YL, Wang JT. Overexpression of CX3CR1 is associated with cellular metastasis, proliferation and survival in GC. Oncol Rep. 2015 Feb;33(2):615-24.
20. Li D, Xia L, Huang P, Wang Z, Guo Q, Huang C, Leng W, Qin S. Cancer-associated fibroblast-secreted IGFBP7 promotes GC by enhancing tumor associated macrophage infiltration via FGF2/FGFR1/PI3K/AKT axis. Cell Death Discov. 2023 Jan 21;9(1):17.

21. Baghery Saghchy Khorasani A, Pourbagheri-Sigaroodi A, Pirsalehi A, Safaroghli-Azar A, Zali MR, Bashash D. The PI3K/Akt/mTOR signaling pathway in GC; from oncogenic variations to the possibilities for pharmacologic interventions. Eur J Pharmacol. 2021 May 5;898:173983.
22. Vivanco I, Sawyers CL. The phosphatidylinositol 3-Kinase AKT pathway in human cancer. Nat Rev Cancer. 2002 Jul;2(7):489-501.
23. Manning BD, Toker A. AKT/PKB Signaling: Navigating the Network. Cell. 2017 Apr 20;169(3):381-405.
24. Porta C, Paglino C, Mosca A. Targeting PI3K/Akt/mTOR Signaling in Cancer. Front Oncol. 2014 Apr 14;4:64.
25. Hoxhaj G, Manning BD. The PI3K-AKT network at the interface of oncogenic signalling and cancer metabolism. Nat Rev Cancer. 2020 Feb;20(2):74-88.
26. Isaac R, Goldstein I, Furth N, Zilber N, Streim S, Boura-Halfon S, Elhanany E, Rotter V, Oren M, Zick Y. TM7SF3, a novel p53-regulated homeostatic factor, attenuates cellular stress and the subsequent induction of the unfolded protein response. Cell Death Differ. 2017 Jan;24(1):132-143.
27. Isaac R, Vinik Y, Mikl M, Nadav-Eliyahu S, Shatz-Azoulay H, Yaakobi A, DeForest N, Majithia AR, Webster NJG, Shav-Tal Y, Elhanany E, Zick Y. A seven-transmembrane protein-TM7SF3, resides in nuclear speckles and regulates alternative splicing. iScience. 2022 Oct 4;25(11):105270.
28. Beck A, Isaac R, Lavelin I, Hart Y, Volberg T, Shatz-Azoulay H, et al. An siRNA screen identifies transmembrane 7 superfamily member 3 (TM7SF3), a seven transmembrane orphan receptor, as an inhibitor of cytokine-induced death of pancreatic beta cells. Diabetologia. 2011 Nov;54(11):2845–55.
29. Binnewies M, Roberts EW, Kersten K, Chan V, Fearon DF, Merad M, Coussens LM, Gabrilovich DI, Ostrand-Rosenberg S, Hedrick CC, Vonderheide RH, Pittet MJ, Jain RK, Zou W, Howcroft TK, Woodhouse EC, Weinberg RA, Krummel MF. Understanding the tumor immune microenvironment (TIME) for effective therapy. Nat Med. 2018 May;24(5):541-550.
30. Chen DS, Mellman I. Elements of cancer immunity and the cancer-immune set point. Nature. 2017 Jan 18;541(7637):321-330.
31. Fridman WH, Zitvogel L, Sautès-Fridman C, Kroemer G. The immune contexture in cancer prognosis and treatment. Nat Rev Clin Oncol. 2017 Dec;14(12):717-734.
32. Hirai H, Sootome H, Nakatsuru Y, Miyama K, Taguchi S, Tsujioka K, Ueno Y, Hatch H, Majumder PK, Pan BS, Kotani H. MK-2206, an allosteric Akt inhibitor, enhances antitumor efficacy by standard chemotherapeutic agents or molecular targeted drugs in vitro and in vivo. Mol Cancer Ther. 2010 Jul;9(7):1956-67.
33. Jo H, Mondal S, Tan D, Nagata E, Takizawa S, Sharma AK, Hou Q, Shanmugasundaram K, Prasad A, Tung JK, Tejeda AO, Man H, Rigby AC, Luo HR. Small molecule-induced cytosolic activation of protein kinase Akt rescues ischemia-elicited neuronal death. Proc Natl Acad Sci U S A. 2012 Jun 26;109(26):10581-6.
34. Hanahan D. Hallmarks of Cancer: New Dimensions. Cancer Discov. 2022 Jan;12(1):31-46.

35. Hetz C, Papa FR. The Unfolded Protein Response and Cell Fate Control. Mol Cell. 2018 Jan 18;69(2):169-181.
36. Urra H, Dufey E, Avril T, Chevet E, Hetz C. Endoplasmic Reticulum Stress and the Hallmarks of Cancer. Trends Cancer. 2016 May;2(5):252-262.
37. Pavlova NN, Thompson CB. The Emerging Hallmarks of Cancer Metabolism. Cell Metab. 2016 Jan 12;23(1):27-47.
38. Negrini S, Gorgoulis VG, Halazonetis TD. Genomic instability--an evolving hallmark of cancer. Nat Rev Mol Cell Biol. 2010 Mar;11(3):220-8.
39. Fruman DA, Chiu H, Hopkins BD, Bagrodia S, Cantley LC, Abraham RT. The PI3K Pathway in Human Disease. Cell. 2017 Aug 10;170(4):605-635.
40. Martini M, De Santis MC, Braccini L, Gulluni F, Hirsch E. PI3K/AKT signaling pathway and cancer: an updated review. Ann Med. 2014 Sep;46(6):372-83.
41. Madhunapantula SV, Mosca PJ, Robertson GP. The Akt signaling pathway: an emerging therapeutic target in malignant melanoma. Cancer Biol Ther. 2011 Dec 15;12(12):1032-49.
42. Cassetta L, Fragkogianni S, Sims AH, Swierczak A, Forrester LM, Zhang H, Soong DYH, Cotechini T, Anur P, Lin EY, Fidanza A, Lopez-Yrigoyen M, Millar MR, Urman A, Ai Z, Spellman PT, Hwang ES, Dixon JM, Wiechmann L, Coussens LM, Smith HO, Pollard JW. Human Tumor-Associated Macrophage and Monocyte Transcriptional Landscapes Reveal Cancer-Specific Reprogramming, Biomarkers, and Therapeutic Targets. Cancer Cell. 2019 Apr 15;35(4):588-602.e10.
43. Noy R, Pollard JW. Tumor-associated macrophages: from mechanisms to therapy. Immunity. 2014 Jul 17;41(1):49-61.
44. Ruffell B, Coussens LM. Macrophages and therapeutic resistance in cancer. Cancer Cell. 2015 Apr 13;27(4):462-72.
45. Vitale I, Manic G, Coussens LM, Kroemer G, Galluzzi L. Macrophages and Metabolism in the Tumor Microenvironment. Cell Metab. 2019 Jul 2;30(1):36-50.
46. Mantovani A, Allavena P, Marchesi F, Garlanda C. Macrophages as tools and targets in cancer therapy. Nat Rev Drug Discov. 2022 Nov;21(11):799-820.
47. Imai T, Hieshima K, Haskell C, Baba M, Nagira M, Nishimura M, Kakizaki M, Takagi S, Nomiyama H, Schall TJ, Yoshie O. Identification and molecular characterization of fractalkine receptor CX3CR1, which mediates both leukocyte migration and adhesion. Cell. 1997 Nov 14;91(4):521-30.
48. Bazan JF, Bacon KB, Hardiman G, Wang W, Soo K, Rossi D, Greaves DR, Zlotnik A, Schall TJ. A new class of membrane-bound chemokine with a CX3C motif. Nature. 1997 Feb 13;385(6617):640-4.
49. Jamieson-Gladney WL, Zhang Y, Fong AM, Meucci O, Fatatis A. The chemokine receptor CX_3CR1 is directly involved in the arrest of breast cancer cells to the skeleton. Breast Cancer Res. 2011 Sep 20;13(5):R91.
50. Caunt CJ, Sale MJ, Smith PD, Cook SJ. MEK1 and MEK2 inhibitors and cancer therapy: the long and winding road. Nat Rev Cancer. 2015 Oct;15(10):577-92.

51. Ebert PJR, Cheung J, Yang Y, McNamara E, Hong R, Moskalenko M, Gould SE, Maecker H, Irving BA, Kim JM, Belvin M, Mellman I. MAP Kinase Inhibition Promotes T Cell and Anti-tumor Activity in Combination with PD-L1 Checkpoint Blockade. Immunity. 2016 Mar 15;44(3):609-621.
52. Hu-Lieskovan S, Mok S, Homet Moreno B, Tsoi J, Robert L, Goedert L, Pinheiro EM, Koya RC, Graeber TG, Comin-Anduix B, Ribas A. Improved antitumor activity of immunotherapy with BRAF and MEK inhibitors in BRAF(V600E) melanoma. Sci Transl Med. 2015 Mar 18;7(279):279ra41.
53. Fedele C, Ran H, Diskin B, Wei W, Jen J, Geer MJ, Araki K, Ozerdem U, Simeone DM, Miller G, Neel BG, Tang KH. SHP2 Inhibition Prevents Adaptive Resistance to MEK Inhibitors in Multiple Cancer Models. Cancer Discov. 2018 Oct;8(10):1237-1249.
54. Ooft SN, Weeber F, Dijkstra KK, McLean CM, Kaing S, van Werkhoven E, Schipper L, Hoes L, Vis DJ, van de Haar J, Prevoo W, Snaebjornsson P, van der Velden D, Klein M, Chalabi M, Boot H, van Leerdam M, Bloemendal HJ, Beerepoot LV, Wessels L, Cuppen E, Clevers H, Voest EE. Patient-derived organoids can predict response to chemotherapy in metastatic colorectal cancer patients. Sci Transl Med. 2019 Oct 9;11(513):eaay2574.
55. Driehuis E, Kretzschmar K, Clevers H. Establishment of patient-derived cancer organoids for drug-screening applications. Nat Protoc. 2020 Oct;15(10):3380-3409. doi: 10.1038/s41596-020-0379-4. Epub 2020 Sep 14. Erratum in: Nat Protoc. 2021 Dec;16(12):5739.

Tables

Table.1 Relationship between TM7SF3 expression and clinicopathological features in patients with GC in TCGA-STAD dataset (n=375). (Cutoff =Average value:19.485, * P<0.05* P<0.05)

Variable	No. of patients (%)			P-Value
	Patients	TM7SF3 High (n=130)	TM7SF3 Low (n=245)	
Age (Year)				0.443
≤60	125	40 (30.8%)	85 (34.7%)	
> 60	250	90 (69.2%)	160 (65.3%)	
Gender				0.726
Male	241	82 (63.1%)	159 (64.9%)	
Female	134	48 (36.9%)	86 (35.1%)	
T stage				0.038*
T1/T2/T3	267	88 (67.7%)	185 (75.5%)	
T4	108	42 (32.3%)	60 (24.5%)	
N stage				0.781
N0	113	38 (29.2%)	75 (30.6%)	
N1/N2/N3	246	92 (70.8%)	170 (69.4%)	
M stage				0.897
M0	330	115 (88.5%)	215 (87.8%)	
M1	25	9 (6.9%)	16 (6.5%)	
Mx	20	6 (4.6%)	14 (5.7%)	
Tumor Grade				0.920
G1	10	3 (2.3%)	7 (2.9%)	
G2	137	45 (34.6%)	92 (37.6%)	
G3	219	79 (60.8%)	140 (57.1%)	
Gx	9	3 (2.3%)	6 (2.4%)	
Tumor Type				0.719
Diffuse	73	23 (17.7%)	50 (20.4%)	
Intestinal	164	56 (43.1%)	108 (44.1%)	
Adenocarcinoma	138	51 (39.2%)	87 (35.5%)	
Tumor Location				0.760
Upper	133	46 (35.4%)	87 (35.5%)	

Middle	90	35 (26.9%)	55 (22.4%)	
Lower	135	44 (33.8%)	91 (37.1%)	
Total	17	5 (3.8%)	12 (4.9%)	
Clinical Stage				0.186
I- II	164	50 (38.5%)	114 (46.5%)	
III-IV	188	69 (53.1%)	119 (48.6%)	
Unknown	23	11 (8.5%)	12 (4.9%)	

Table.2 Multivariate analysis of the clinicopathological factors on the expression of TM7SF3 gene and clinical prognosis for GC patients in Kaplan-Meier plotter database.

Clinicopathological Characteristics	GSE15459 (222477_at)/OS			GSE14210 (217974_at)/OS		
	N	Hazard Ratio (HR)	P-value	N	Hazard Ratio (HR)	P-value
Gender						
Female	68	1.20 (0.54-2.70)	0.651	22	1.01 (0.38-2.68)	0.987
Male	127	1.49 (0.85-2.59)	0.158	96	1.32 (0.87-2.01)	0.195
Clinical Stage						
I	32	0.37 (0.09-1.49)	0.146	–	–	–
II	30	1.83 (0.47-7.08)	0.376	–	–	–
III	71	1.58 (0.82-3.03)	0.166	–	–	–
IV	62	0.70 (0.38-1.28)	0.243	–	–	–
T Stage						
T1	11	–	–	–	–	–
T2	44	1.67 (0.48- 5.87)	0.418	–	–	–
T3	101	2.02 (1.21-3.35)	0.0057*	–	–	–
T4	15	–	–	–	–	–
N Stage						
N0	38	1.46 (0.50-4.20)	0.486	–	–	–
N1	72	1.30 (0.60-2.84)	0.506	–	–	–
N2	36	1.68 (0.70-4.00)	0.238	–	–	–
N3	24	1.49 (0.55-4.05)	0.430	–	–	–
N1+N2+N3	132	1.33 (0.84-2.12)	0.223	–	–	–
M Stage						
M0	144	1.36 (0.79-2.34)	0.266	–	–	–
M1	30	2.16 (0.86-5.45)	0.094	–	–	–
Lauren-Classification						
Intestinal	100	1.07 (0.60-1.89)	0.822	–	–	–
Diffuse	76	1.76 (0.78- 3.97)	0.165	–	–	–
Mixed	21	1.89 (0.53-6.73)	0.320	–	–	–
Differentiation						

Well	5	—	—	—	—	—
Moderately	67	1.09 (0.54-2.23)	0.804	—	—	—
Poorly	121	1.76 (1.06-2.93)	0.026*	—	—	—
HER2 Status						
Positive	89	0.92 (0.49-1.72)	0.787	66	1.87 (1.09-3.21)	0.021*
Negative	108	1.77 (0.97-3.23)	0.061	52	1.45 (0.77-2.73)	0.246
Treatment						
Surgery alone	131	1.17 (0.66-2.08)	0.587	0	—	—
5-FU based adjuvant	34	1.84 (0.72-4.71)	0.195	118	1.56 (1.05-2.34)	0.028*
Other adjuvants	0	—	—	0	—	—

* P<0.05 means significantly.

Table.3 The correlation analysis between TM7SF3 expression and gene markers of various immune cells in TIMER- STAD dataset.

Immune Cells	Gene Markers	STAD			
		None		Tumor Purity-Adjusted	
		Cor. R	P-Value	Cor. R	P-Value
CD4+T cell	CD4	0.249	3.2e-07***	0.290	8.59e-09***
CD8+ T cell	CD8A	0.182	1.96e-04***	0.214	2.72e-05***
T cell exhaustion	PD-1 (PDCD1)	0.131	7.51e-03**	0.162	1.51e-03**
	CTLA4	0.157	1.31e-03**	0.193	1.55e-04***
	LAG3	0.193	8.01e-05***	0.227	8.30e-06***
	TIM-3(HAVCR2)	0.309	1.57e-10***	0.342	7.65e-12***
	GZMB	0.220	6.42e-06***	0.258	3.43e-07***
	GZMA	0.230	2.43e-06***	0.266	1.41e-07***
B cell	CD19	-0.039	0.432	-0.015	0.775
Monocyte	CD86	0.240	7.25e-07***	0.288	1.08e-08***
	CD115 (CSF1R)	0.287	3.01e-09***	0.319	1.97e-10***
Neutrophils	CD66b (CEACAM8)	0.053	0.285	0.067	0.194
	CD11b (ITGAM)	0.281	6.65e-09***	0.302	2.06e-09***
TAM	CD68	0.249	2.95e-07***	0.261	2.61e-07***
	CD40	0.083	0.0899	0.105	0.0404*
M1 Macrophage	INOS (NOS2)	-0.033	0.506	-0.016	0.758
	CD86	0.240	7.25e-07***	0.288	1.08e-08***
M2 Macrophage	CD163	0.336	2.88e-12***	0.359	6.12e-13***
	CD206 (MRC1)	0.296	9.03e-10***	0.310	6.91e-10***
NK cell	KIR2DL1	0.150	2.23e-03**	0.189	2.14e-04***
	KIR2DL3	0.146	2.91e-03**	0.174	6.75e-04***
	KIR2DL4	0.220	6.3e-06***	0.247	1.10e-06***
Dendritic cell	HLA-DPB1	0.143	3.44e-03**	0.186	2.68e-04***
	HLA-DQB1	0.104	0.0345*	0.143	5.40e-03**
	HLA-DRA	0.201	3.69e-05***	0.237	3.03e-06***
Th1	IFN-γ (IFNG)	0.263	5.7e-08***	0.294	5.43e-09***

	TNF-α (TNF)	0.004	0.94	0.025	0.630
Th2	GATA3	0.065	0.188	0.107	3.80e-02*
	IL13	0.020	0.691	0.033	0.518
Tfh	IL21	0.203	3.09e-05***	0.211	3.61e-05***
Th17	IL17A	-0.036	0.469	-0.022	0.670
Treg	FOXP3	0.159	1.16e-03**	0.198	1.04e-04***

Cor, R value of Spearman's correlation; None, correlation without adjustment. Purity, correlation adjusted by purity. *P < 0.05; **P < 0.01; ***P < 0.001. STAD, stomach adenocarcinoma; TAM, tumor-associated macrophage; Tfh, follicular helper T cell; Th, T helper cell; Treg, regulatory T cell. NK cell, Natural Killer cell

Figures

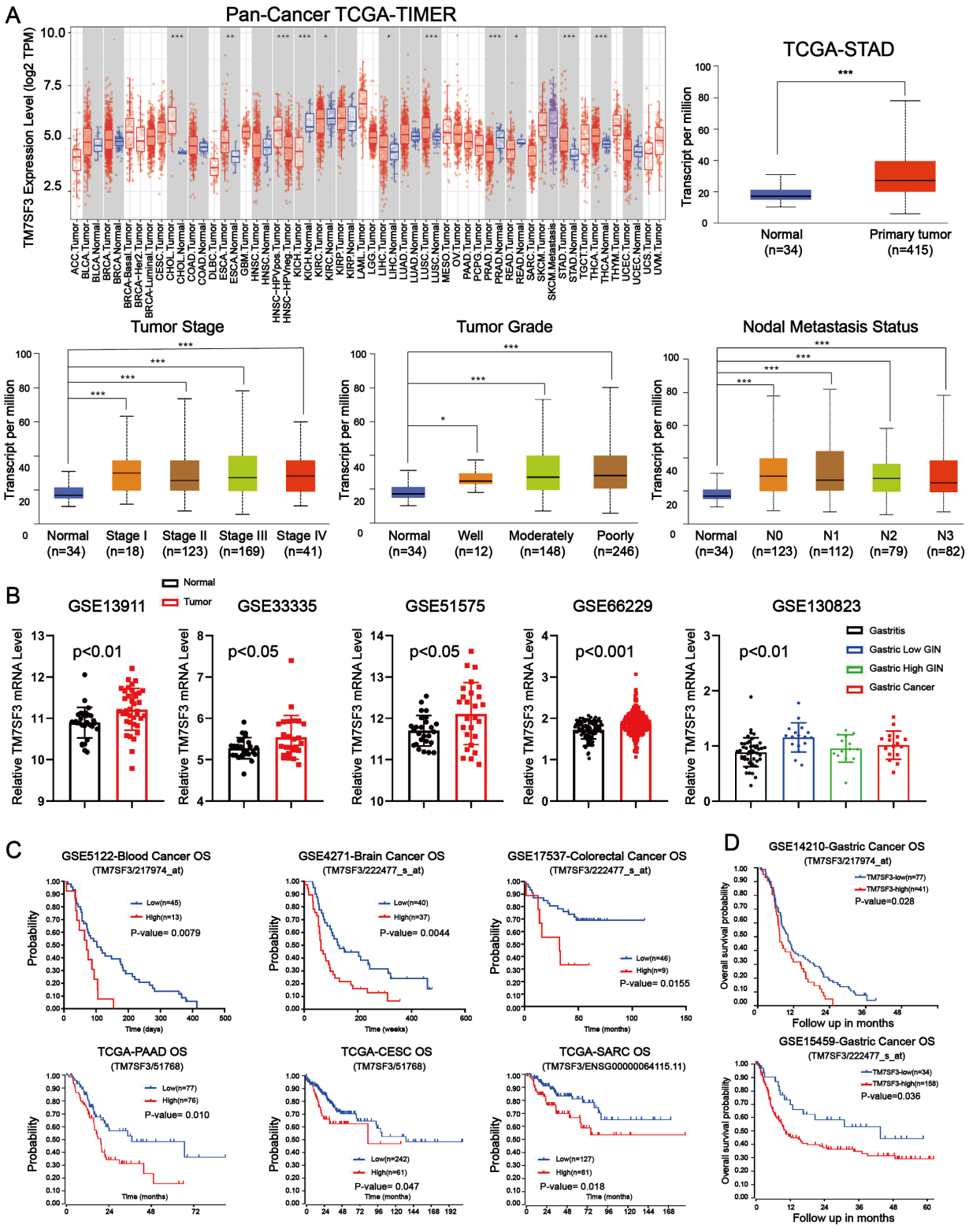


Figure 1

The expression level of TM7SF3 in GC. (A) The expression level of TM7SF3 in normal gastric mucosal tissue and GC tissue. The relationship of TM7SF3 expression and tumor stage, tumor grade, and lymph node metastasis status in TCGA-STAD dataset. (B) The expression level of TM7SF3 mRNA in GC tissues

and corresponding normal tissues based on GEO datasets in GC patients. (C) The description of survival curves of overall survival time (OS) in the patients with blood cancer, brain cancer, colorectal cancer, pancreatic cancer, cervical squamous cell carcinoma and sarcoma based on the GEO and TCGA datasets. (D) Survival analysis of OS for these patients from three GC-patient cohorts in GEO datasets.

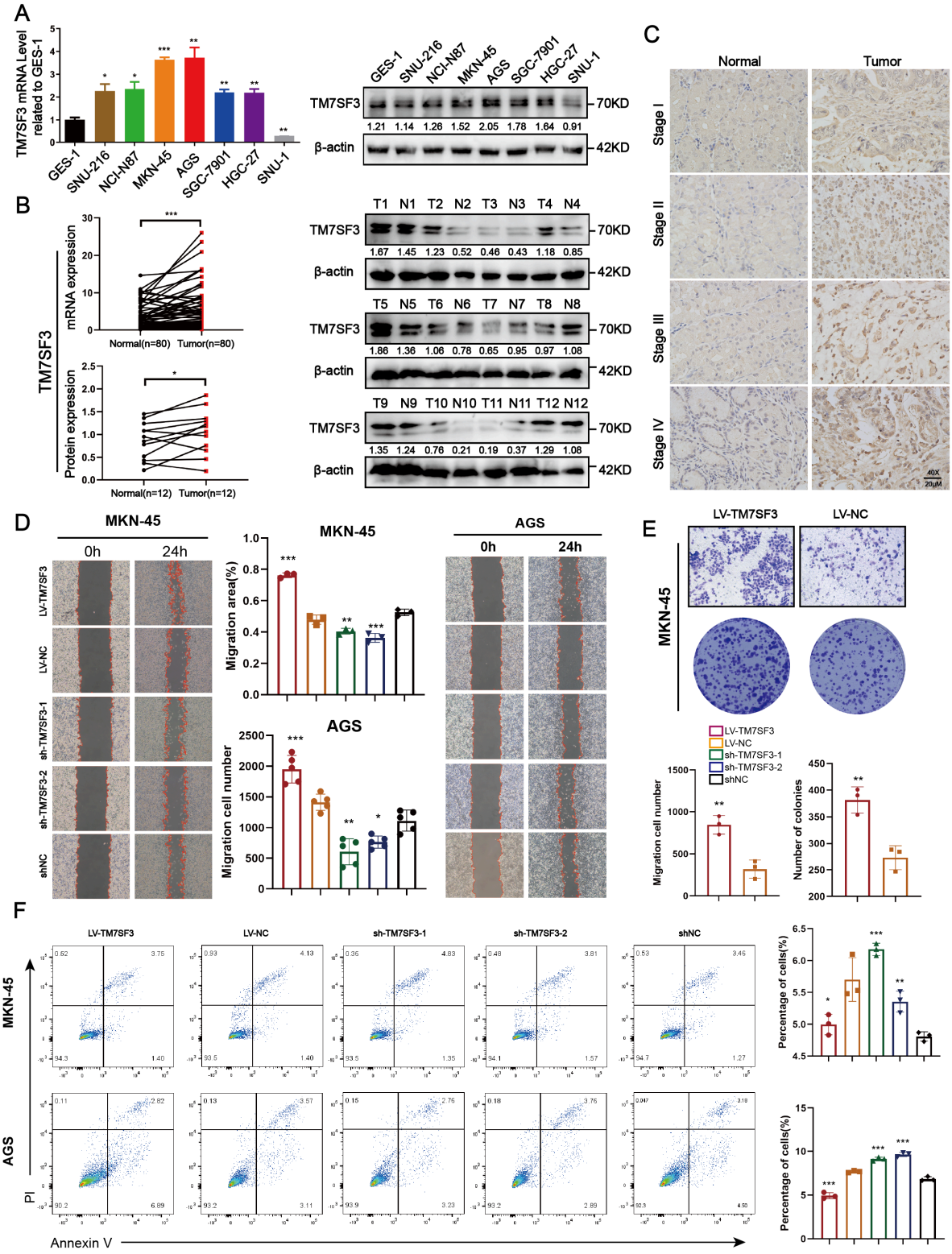


Figure 2

TMS7F3 is highly expressed in GC and promotes the proliferation and migration of GC cells. (A) TM7SF3 mRNA expression and protein levels in different GC cell lines. (B) The mRNA and protein expression level of TM7SF3 in the adjacent normal gastric tissues and tumor tissues. (C) Immunohistochemical staining was performed to compare tumor tissue with normal tissue at different tumor stages, Scale bar:40x: 20μM. (D-E) Results of scratch assays, invasion assays, and colony formation assays. (F) Total apoptosis rates of MKN-45 and AGS cells(n = 3).

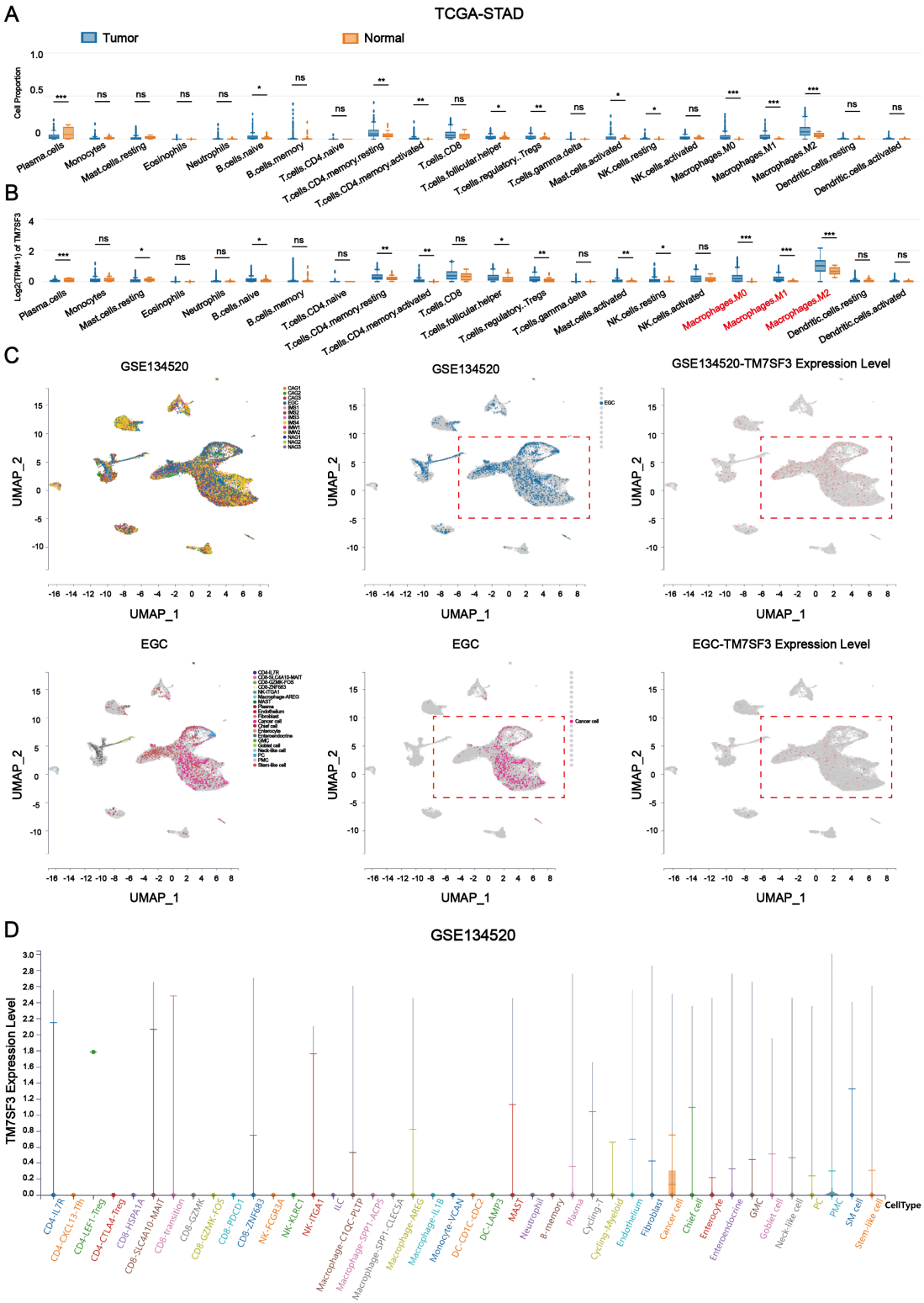


Figure 3

The relationship between TM7SF3 expression level and immune infiltration of tumor tissues and paired normal tissues in GC patients from TCGA-STAD dataset. (A) The cell ratios of diverse immune cell populations of the tumor tissues and paired normal tissues according to the analysis from the TCGA-STAD dataset. (B) Differences of TM7SF3 mRNA expression and the proportions of diverse immune cell populations between tumors and paired normal tissues according to the analysis from the TCGA-STAD dataset. (C) Comprehensive analysis of the distribution and expression of the TM7SF3 gene and different cell subsets in a GC-related single-cell sequencing dataset GSE134520. (D)The abundance of TM7SF3 expression level in various types of cells in the GSE134520 dataset.

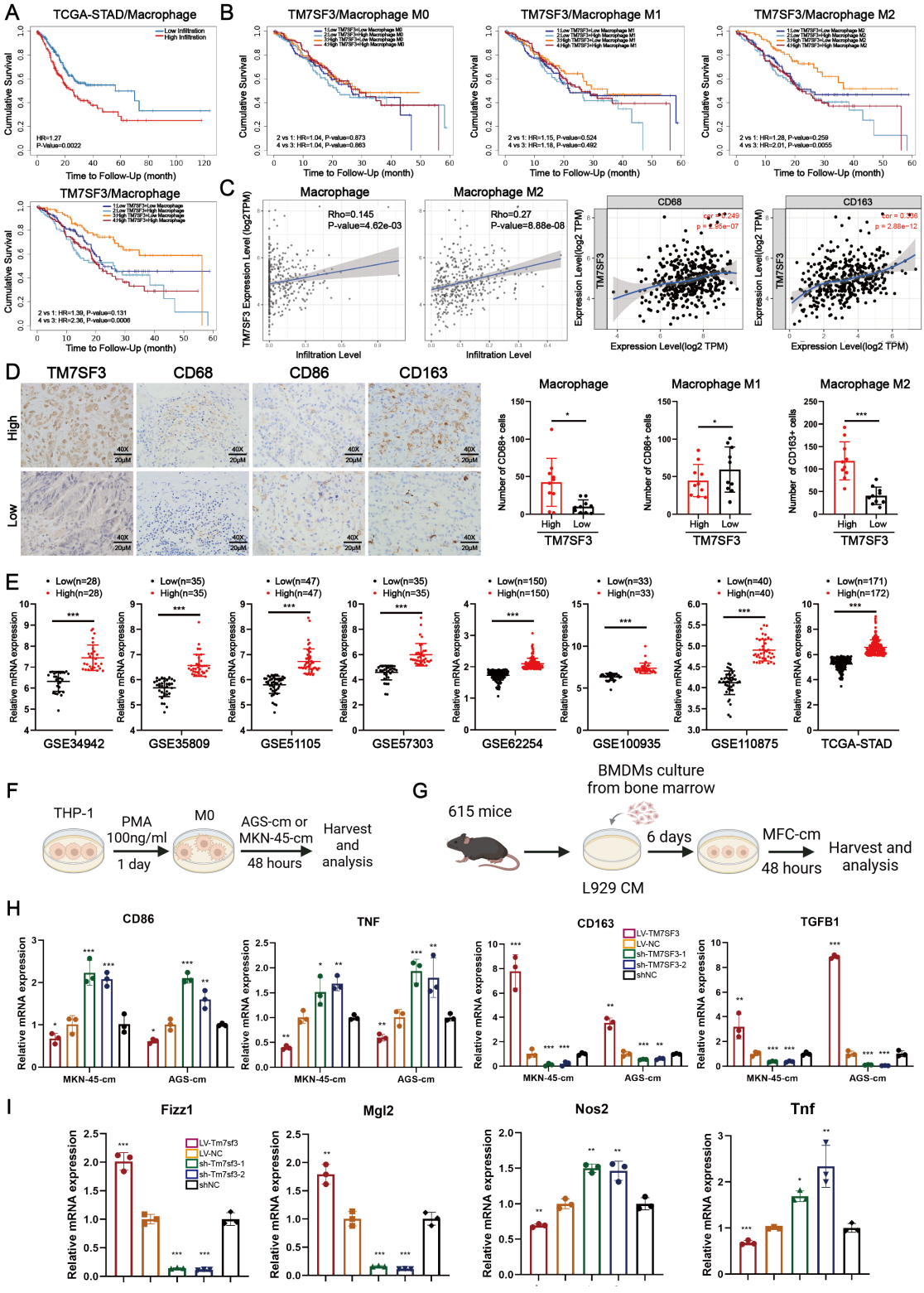


Figure 4

The relationship of TM7SF3 expression and macrophage M2 polarisation in GC. (A) Survival analysis of TM7SF3 expression with high and low macrophage infiltration in the TCGA-STAD database. (B) Survival curves of TM7SF3 expression and different subtypes of macrophage infiltration in GC based on a TIMER database analysis. (C) The correlation between TM7SF3 expression and the infiltration level and gene markers of macrophage and M2 macrophage according to the TIMER database analysis. (D) IHC of

TM7SF3 and macrophage-related marker CD68, CD86 and CD163 expression, Scale bar:40x: 20μM. (E) Using GSEA to explore the interaction between TM7SF3 and macrophage in these GC-GEO datasets, which were averagely divided into two groups according to the expression level of TM7SF3. (F-G) Experimental design. (H) THP-1 cells were induced to differentiate into M0 macrophages with PMA (100 ng/mL) for 1 day and cultured with MKN-45 and AGS cells conditioned medium for 48 hours. The expression levels of M2 markers (CD163, TGFB1) and M1 markers (CD86, TNF) were measured by qRT-PCR. (I) Bone marrow cells from 615 mice were extracted in vitro and induced into BMDMs using L929 cells conditioned medium (L929-cm). After 6 days, the macrophages were cultured in MFC cells conditioned medium (MFC-cm) for 48 hours. The expression levels of M2 markers (Fizz1, Mgl2) and M1 markers (Nos2, Tnf) were measured by qRT-PCR. IHC, immunohistochemistry.

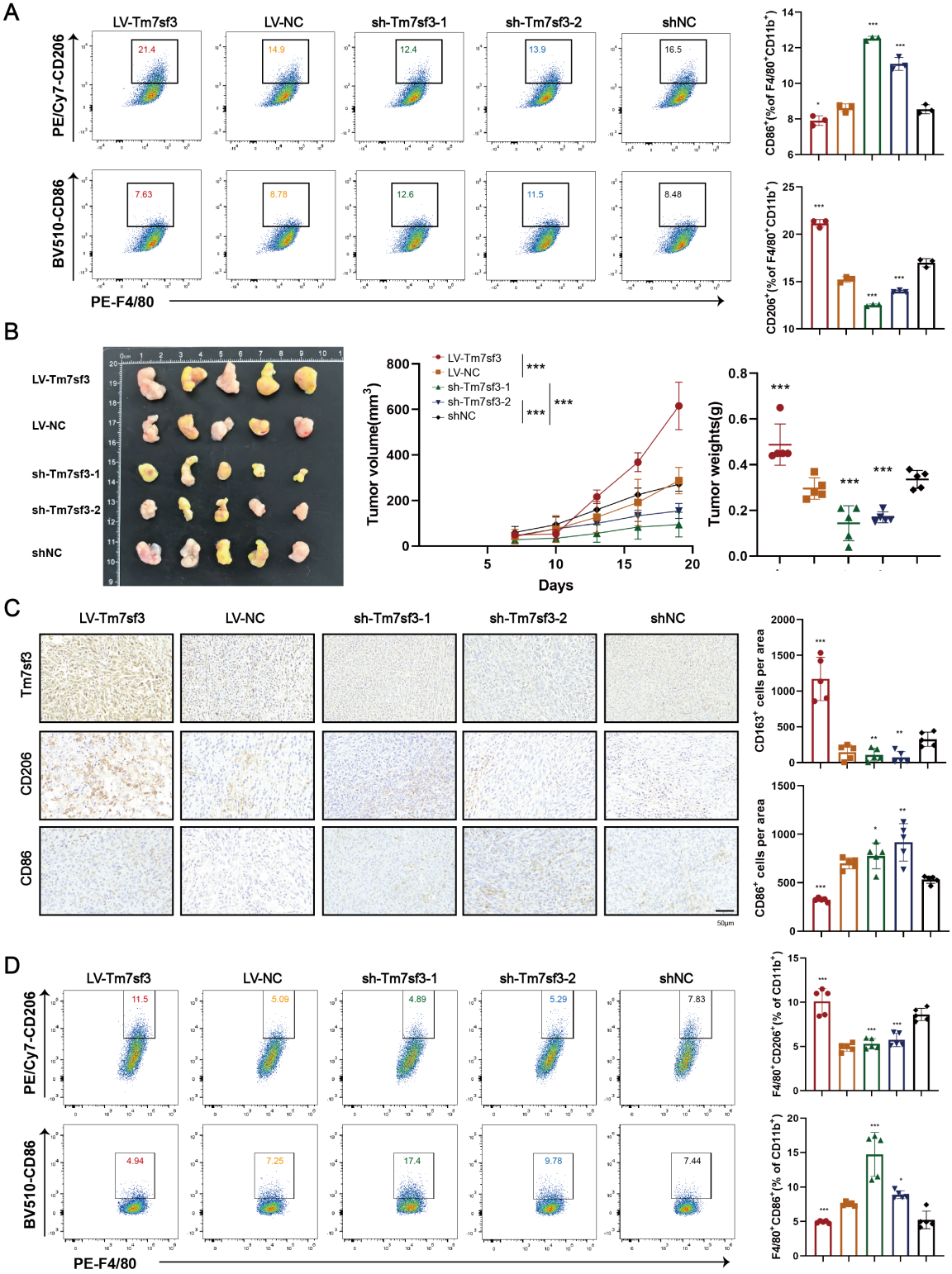


Figure 5

TM7SF3 promotes M2 macrophage polarisation in vivo and in vitro. (A) Bone marrow cells from 615 mice were extracted in vitro and induced into BMDMs using L929 cells conditioned medium (L929-cm). After 6 days, the macrophages were cultured in MFC cells conditioned medium (MFC-cm) for 48 hours. The proportion of M2 macrophages in each group of macrophages was detected by flow cytometry. (B) Left: MFC cells (1×10^6) were transplated subcetaneously (s.c.) into 615 mice (n=5/group). Right: Tumour

growth and weights. IHC staining with CD206, CD86, Tm7sf3-specific antibodies to detect $CD206^+$ and $CD86^+$ macrophage infiltration in subcutaneously transplanted MFC tumours (n=5/group). (C)The number of CD206, CD86, Tm7sf3 positive cells was counted in subcutaneous tumour sections from each group of mice. Five random areas were selected for analysis on each slide. Scale bar:40×: 50μM (D) FACS analysis of the $CD206^+$ and $CD86^+$ macrophages in MFC tumours (n=5/group). FACS, flow cytometry; IHC, immunohistochemistry.

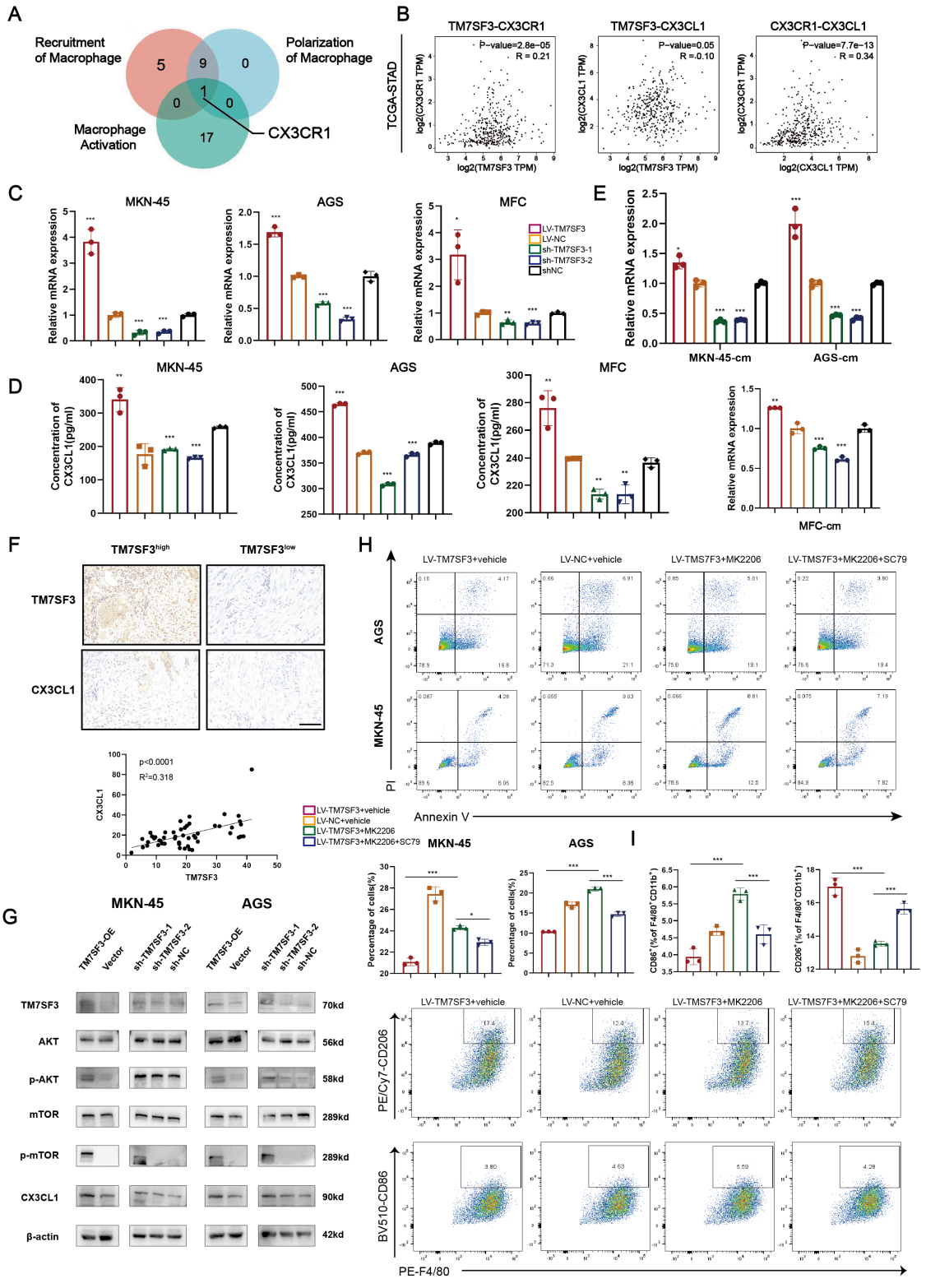


Figure 6

TM7SF3 activates the PI3K/AKT signaling pathway to induce CX3CL1 expression and promote macrophage M2 polarization in GC. (A) Venn diagram illustrating the overlap of genes involved in macrophage recruitment, activation, and M2 polarization. (B) Correlation analysis of TM7SF3, CX3CR1, and CX3CL1 expression in the TCGA-STAD dataset. (C-D) Relative expression of the CX3CL1 determined by qRT-PCR and ELISA. (E) CX3CR1 expression of THP-1 and BMDMs cultures with MKN-45-cm, AGS-cm and MFC-cm detected by qRT-PCR. (F) Correlation analysis of IHC staining of GC tissues between TM7SF3 and CX3CL1 protein expression ($n = 50$, $R^2 = 0.318$, $P < 0.0001$). Scale bar:40×: 50μM (G) Western blotting to detect the expression of p-AKT (Ser473), AKT, p-mTOR (Ser2448), mTOR, CX3CL1 and β-actin. (H) Total apoptosis rates of GC cells treated with MK2206 (10 μM) and SC79 (10 μM) for 24h were analyzed. (I) Flow cytometric analysis of CD206 and CD86 expression in BMDMs cultured with cultured medium of MFC cells treated with MK2206 and SC79. IHC, immunohistochemistry.

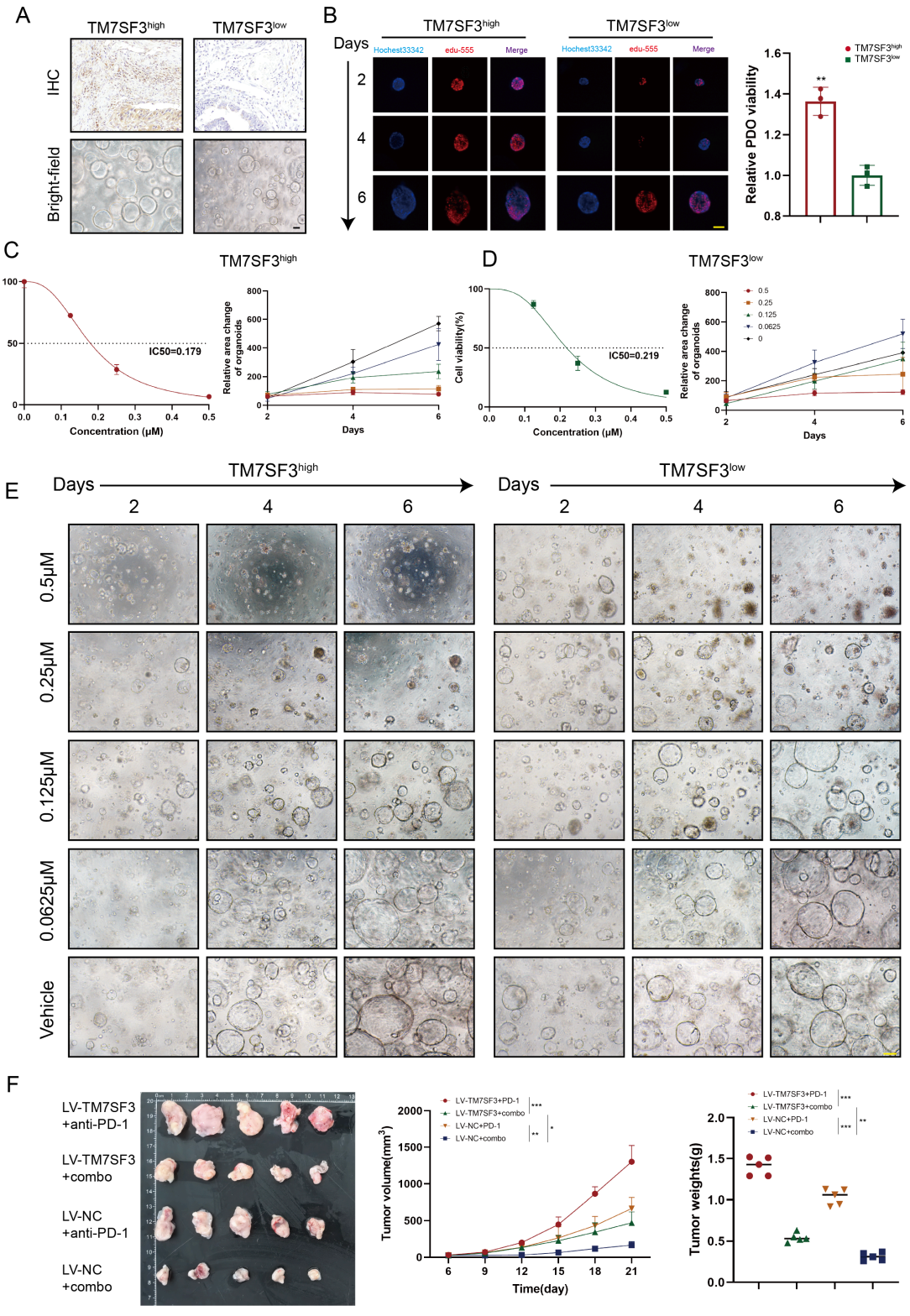


Figure 7

TM7SF3 expression predicts the therapeutic response of GC patient-derived organoids (PDOs) to Trametinib and combination immunotherapy. (A) Representative immunohistochemical (IHC) staining of TM7SF3 in GC tissues and corresponding bright-field images of patient-derived organoids (PDOs) established from tumors with high or low TM7SF3 expression. (B) Representative EdU staining images of $TM7SF3^{high}$ and $TM7SF3^{low}$ PDOs cultured for 2, 4 and 6 days. Scale bar:10×: 100μM. (C-E) Dose-

response curve of Trametinib in TM7SF3^{high} and TM7SF3^{low} PDOs. Growth curves of PDOs treated with increasing concentrations of Trametinib (0, 0.0625, 0.125, 0.25 and 0.5 μM) over 6 days, represented as relative organoid area. Scale bar:10×: 100μM (F) Tumour growth of MFC tumour-bearing mice , treated with an anti-PD-1 mAb (5 mg/kg) and the anti-PD-1 mAb (5 mg/kg) combined with the trametinib (1 mg/kg). Treatment is administered every three days, starting from
the sixth day (n=5/group).

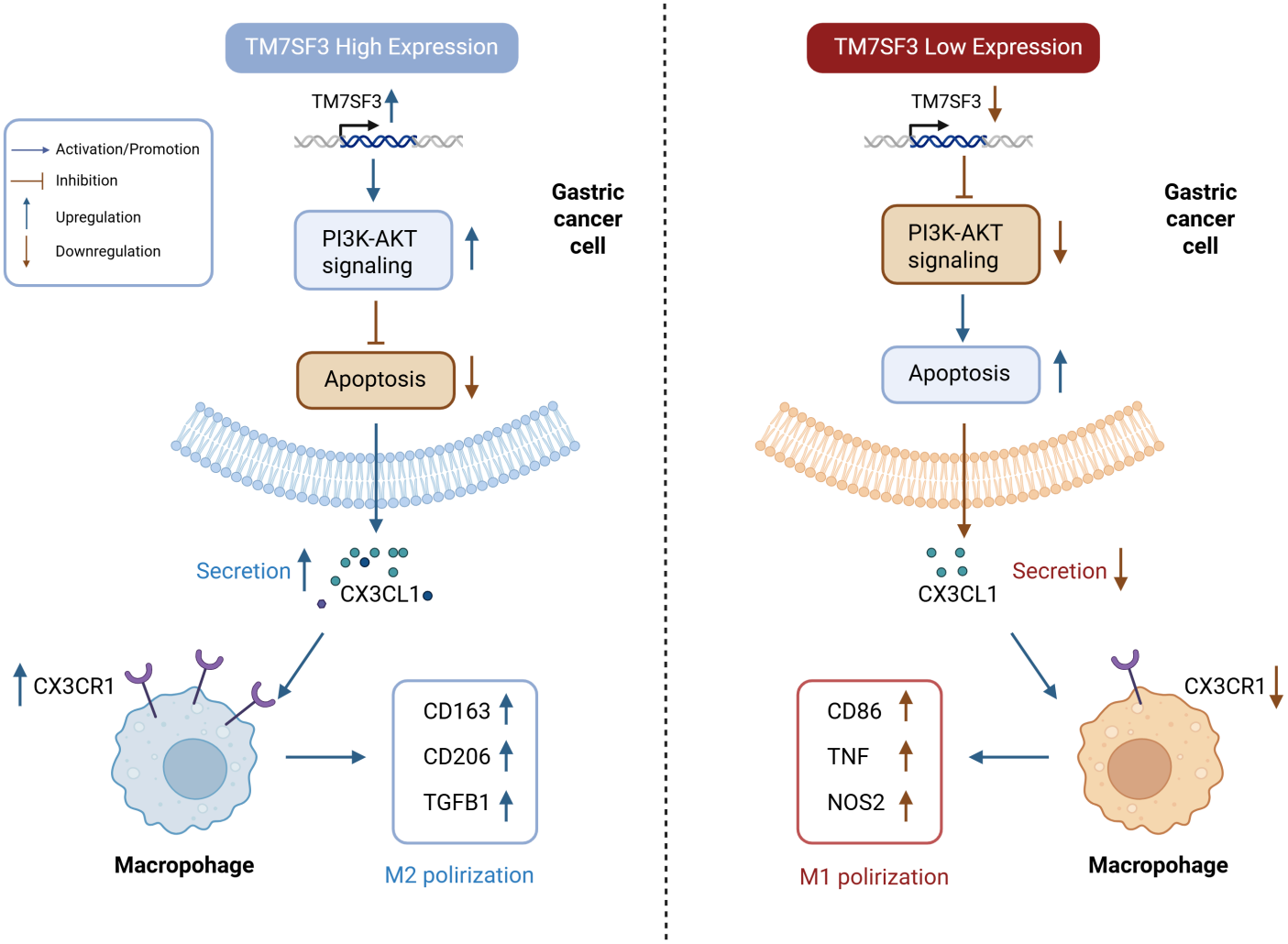


Figure 8

TM7SF3 suppresses PI3K-AKT signaling, declines apoptosis, increases CX3CL1 secretion, and promotes M2 macrophage polarization through CX3CL1/CX3CR1 signaling.

Supplementary Files

This is a list of supplementary files associated with this preprint. Click to download.

- SupplementaryFigure1.png
- SupplementaryFigure2.png

- SupplementaryFigure3.tif
- SupplementaryFigure4.tif
- SupplementaryFigure5.png
- SupplementaryFigure6.png
- SupplementaryMaterials.docx
- SupplementaryTable1.docx
- SupplementaryTable2.docx
- SupplementaryTable3.docx